November 27, 1991
CO-RDFR

Large Coherent Arrays for Laser Radars
Phase I

R&D FINAL REPORT

Prepared for: ONR
Arlington, VA 22217

Contract No: N00014-91-C-0150

Prepared by: INTERSPEC Incorporated
110 West Butler Avenue
Ambler, PA 19002-5795

Report Prepared by: Hesham Attia, Ph.D.
(215) 540-9190, Ext. 1806

November 27, 1991
CO-RDFR

Large Coherent Arrays for Laser Radars
Phase I

R&D FINAL REPORT

Prepared for: ONR
Arlington, VA 22217

Contract No: N00014-91-C-0150

Prepared by: INTERSPEC Incorporated
110 West Butler Avenue
Ambler, PA 19002-5795

Report Prepared by: Hesham Attia, Ph.D.
(215) 540-9190, Ext. 1806

Statement A per telecon
Dr. William Miceli ONR/Code 1264
Arlington, VA 22217-5000

NWW 1/21/92

SECURITY CLASSIFICATION OF THIS PAGE (When Data Entered)

REPORT DOCUMENTATION PAGE	READ INSTRUCTIONS BEFORE COMPLETING FORM
1. REPORT NUMBER	2. GOVT ACCESSION NO. / 3. RECIPIENT'S CATALOG NUMBER
4. TITLE (and Subtitle) Large Coherent Arrays For Laser Radars Phase I	5. TYPE OF REPORT & PERIOD COVERED Final Technical Report 6. PERFORMING ORG. REPORT NUMBER
7. AUTHOR(s) E. Hesham Attia	8. CONTRACT OR GRANT NUMBER(s) N00014-91-C-0150
9. PERFORMING ORGANIZATION NAME AND ADDRESS Interspec, Inc. 110 W. Butler Ave. Ambler, PA 19002	10. PROGRAM ELEMENT, PROJECT, TASK AREA & WORK UNIT NUMBERS
11. CONTROLLING OFFICE NAME AND ADDRESS ONR Arlington, VA 22217	12. REPORT DATE November 1991 13. NUMBER OF PAGES 62
14. MONITORING AGENCY NAME & ADDRESS(if different from Controlling Office)	15. SECURITY CLASS. (of this report) Unclassified 15a. DECLASSIFICATION/DOWNGRADING SCHEDULE
16. DISTRIBUTION STATEMENT (of this Report)	
17. DISTRIBUTION STATEMENT (of the abstract entered in Block 20, if different from Report)	
18. SUPPLEMENTARY NOTES	
19. KEY WORDS (Continue on reverse side if necessary and identify by block number) Lidar, Laser Radar, Phased Array Lindar, Self-Cohering, Self-Phasing, Self-Calibration, Large Aperture, Coherent Optical Arrays	

20. ABSTRACT (Continue on reverse side if necessary and identify by block number)

A bistatic laser radar with a large, sparse, phased array, receive aperture has been previously proposed for various critical strategic defense applications such as discrimination, target tracking, pointing, and fire control. The same concept could also be applied to the difficult problem of theater missile defense (TMD) using an airborne platform (above any cloud cover). The basic problem is to ensure that the outputs of the receive subapertures

DD FORM 1 JAN 73 1473 EDITION OF 1 NOV 65 IS OBSOLETE

are coherently combined in order to obtain the desired phased array performance. The general approach previously taken relaxes the tolerances on the locations of array elements and tries to compensate for the resulting phase errors adaptively, by phase conjugating returns from a "phase-up" source of opportunity found within the target area. We recognized this procedure as the simplest among a class of "self-cohering" techniques that **Interspec** has developed in the past decade for the purpose of obtaining diffraction-limited performance from distorted apertures for radar applications. In this effort, we adapted and applied a powerful self-cohering technique to this problem. This advanced technique offers significantly better reliability and performance compared to currently employed simple phase conjugation of a phase-up source of opportunity or other related methods.

Most of our algorithmic work during this effort has focused on extending the Spatial Correlation Algorithm (SCA) to two-dimensional array geometries. The SCA predicts and corrects aperture distortion using the spatial correlation properties of target returns. We realized that the SCA is the most promising of all existing self-cohering techniques because of its ability to correct arbitrarily large phase errors that can be totally independent from one array element to another without requiring a phase-up source. Instead, a number of independent looks from the target are needed. These looks, needed for estimating the required correlations, can be obtained via either of the following two methods (or by a combination of both):

(1) By range diversity. That is, if the laser radar can resolve the target into a number of range cells, then each range cell will provide an independent look.

(2) By rotation diversity. A rotating target with a diffuse surface will provide a number of independent looks while being observed over time. Because of the short optical wavelengths involved, a minute rotation from pulse to pulse is sufficient to decorrelate the looks.

The weighted least squares (minimum variance) 2-D SCA, we developed, provides the *optimal* solution to the problem. Combined with our new phase-unwrapping techniques and symmetric phase constraint, our solution is *direct*, in the sense that it works on all differential phase measurements at the same time. Moreover, we analyzed and predicted the performance of our newly developed algorithms. Performance predictions are very promising. Performance curves show that a 5×5 array trying to image an extended target (consisting of 3×3 speckles) at a signal to noise ratio of 0 dB per element per look (with a total of 20 available looks) will only suffer a 1 dB loss in the normalized mainlobe gain of its point spread function after applying our optimal solution. Computer simulations verified this result.

This Phase I SBIR study leads to a Phase II where we propose to build an experimental 10×10 heterodyne array, and use it in order to demonstrate the validity and performance of our advanced self-cohering techniques under realistic conditions. This experimental set-up will allow us to:

(1) Introduce true mechanical errors.

(2) Experiment with different array geometries.

(3) Introduce vibrations within the array. This can simulate an airborne system for a Theater Missile Defense (TMD) scenario.

(4) Image a target through significant atmospheric turbulence (for possible TMD applications).

CONTENTS

0.0 REPORT SUMMARY

0.1 Objectives

Phase I of this SBIR was awarded by SDIO (through ONR) with an effective date of June 1, 1991. The main objective was to determine the feasibility of applying our advanced self-cohering techniques to the large-aperture, coherent array lidar problem. Specifically, we had the following objectives:

(1) To adapt a number of our advanced self-cohering techniques to large-aperture coherent array lidar.

(2) To evaluate and quantify the improvements offered by our techniques.

The tasks performed under this effort are:

(1) Baseline Development

(2) Adaptation of Modern Self-Cohering Techniques

(3) Prediction of Expected Performance, and

(4) Design of a Phase II Experiment.

Discussions with Dr. Stuart Clark, Loughborough University, United Kingdom, currently working at US Naval Weapons Center, China Lake, CA, has resulted in a series of recommendations to best use resources under this contract. In a letter from Dr. Louis DeSandare of NWC to Dr. William Miceli of the ONR, it was recommended that Task 1 be de-emphasized and we make use of the results of existing study reports issued by MIT Lincoln Laboratory to establish a set of performance goals. These goals were relayed to us by both Dr. Clark and Dr. DeSandre.

0.2 Technical Problems

A bistatic laser radar with a large, sparse, phased array, receive aperture has been previously proposed for various critical strategic defense applications. The basic problem is to ensure that the outputs of the receive subapertures are coherently combined in order to obtain the desired phased array performance. The general approach previously taken relaxes the tolerances on the locations of array elements and tries to compensate for the resulting phase errors adaptively, by phase conjugating returns from a "phase-up" source of opportunity found within the target area. We recognized this procedure as the simplest

among a class of "self-cohering" techniques that **Interspec** has developed in the past decade for the purpose of obtaining diffraction-limited performance from distorted apertures for radar applications. This SBIR effort adapts and applies a number of innovative self-cohering techniques to this problem. These advanced techniques offer significantly better reliability and performance compared to currently employed simple phase conjugation of a phase-up source of opportunity.

Space-based large aperture laser radars are expected to play an important role in discrimination, target tracking, pointing, and fire control for strategic defense. The same concept could also be applied to the difficult problem of theater missile defense (TMD) using an airborne platform. Our advanced self-cohering techniques will significantly enhance the reliability, angular resolution, and detection performance of large aperture coherent optical arrays.

0.3 General Methodology

Our general methodology has been mostly analytical. We have also closely supported our analytical effort by extensive computer simulations in order to check the validity of our algorithms and theoretical performance predictions. Moreover, some of our ideas have been demonstrated using the existing experimental system at the Naval Weapons Center, China Lake, California.

0.4 Technical Results

The main result of this Phase I SBIR study is that "self-phasing" of a large receive array of optical subaprtures is quite feasible using our advanced "self-cohering" techniques. That is, it is possible, for a bistatic laser radar system, to obtain diffraction-limited performance from a badly distorted, large, optical receive aperture adaptively (using returns from the target area). No strong phase-up point source is required. Instead, a number of independent "looks" from the target are needed. These looks can be obtained via either of the following two methods (or by a combination of both):

(1) By range diversity. That is, if the laser radar can resolve the target into a number of range cells, then each target range cell will provide us with an independent look.

(2) By rotation diversity. A rotating target with a diffuse surface will provide us with a number of independent looks as we observe it over time. Because of the short optical wavelengths involved, a small rotation from pulse to pulse is sufficient to decorrelate the looks.

During the course of this study, we developed a number of advanced self-cohering techniques suited to the problem. In particular, we developed:

(1) Least squares two-dimensional (2-D) SCA.

(2) Weighted least squares (minimum variance) 2-D SCA.

(3) The SCA as a "multiple scatterer algorithm".

The first two techniques can be considered as extensions of the Spatial Correlation Algorithm (SCA) to two-dimensional array geometries. The second algorithm provides the *optimal* solution to the problem given a reasonable number of looks. For the case where we have a limited number of looks and some of which contain dominant scatterers, the third technique exploits these special looks in order to achieve effective self-cohering.

All three techniques solve a set of overdetermined equations relating array distortion to phase measurements. The solutions take on the general form

$$\underline{\delta} = W\underline{\Psi}, \tag{0.1}$$

where $\underline{\delta}$ is the vector of phase corrections, W is a weighting matrix, and $\underline{\Psi}$ is the vector of differential phase measurements.

We developed a symmetric phase constraint that resulted in a symmetric solution amenable to fast matrix inversion algorithms (needed for computing W). Notice that the optimal weights, W, can be precomputed and stored in a look-up table for a given system. Because the solution is symmetric, a small fraction of the entries of W has to actually be computed and stored.

Phase-unwrapping of $\underline{\Psi}$ is essential before applying (0.1). We developed the following methods of phase-unwrapping:

(a) Direct phase-unwrapping.

(b) Generalized, iterative phasor method.

Both methods, (a) and (b), require an initial solution for array phase corrections. We developed two techniques for obtaining such an initial solution (see Section 2.3.4):

(i) Direct integration of phase differences starting from an element near array center and moving outwards (radially) in all directions (quickest method).

(ii) Sequential near-optimal/optimal solutions for subarrays of growing size (most reliable method).

We analyzed and predicted the performance of our newly developed algorithms. Performance predictions are very promising (predicted performance meets and exceeds the goals

set by the staff of the Naval Weapons Center (NWC), China Lake, California). Performance curves show that a 5×5 array trying to image an extended target (consisting of 3×3 speckles) at a signal to noise ratio of 0 dB per element per look (with a total of 20 available looks) will only suffer a 1 dB loss in the normalized mainlobe gain of its point spread function after applying our optimal solution. Computer simulations verified this result. To the best of our knowledge, such performance is unprecedented.

In general, extensive computer simulations have verified all our algorithms and performance predictions.

We have also designed two sets of Phase II experiments for the purpose of demonstrating our advanced self-cohering techniques:

(1) Using the NWC experimental system:

  (1.1) A number of useful experiments can be performed with existing hardware.

  (1.2) On the other hand, the existing CCD array has a very low bandwidth and offers no significant geometrical flexibility.

(2) Building a 10×10 array of individual detectors. This approach makes it possible to test our techniques under realistic conditions. Such an experimental set-up will enable us to:

  (1) Introduce true mechanical errors.

  (2) Experiment with different array geometries.

  (3) Introduce vibrations within the array. This can simulate an airborne system (above the clouds) for a Theater Missile Defense (TMD) scenario.

  (4) Image a target through significant atmospheric turbulence (for possible TMD applications).

  (5) Upgrade the working bandwidth of the system by upgrading the data acquisition and data transfer systems.

0.5 Important Findings and Conclusions

The main result of this Phase I SBIR study is that "self-phasing" of a large receive array of optical subaprtures is quite feasible using our advanced "self-cohering" techniques. That is, it is possible, for a bistatic laser radar system, to obtain diffraction-limited performance from a badly distorted, large, optical receive aperture adaptively (using returns from the target area). No strong phase-up point source is required.

During the course of this study, we developed a number of advanced self-cohering techniques suited to the problem. In particular, we developed:

(1) Least squares two-dimensional (2-D) SCA.

(2) Weighted least squares (minimum variance) 2-D SCA.

(3) The SCA as a "multiple scatterer algorithm".

It should be noted that the second algorithm provides the *optimal* solution to the problem given a reasonable number of looks.

Also, we developed a symmetric phase constraint that resulted in a symmetric solution amenable to fast matrix inversion algorithms. The optimal weighting matrix, W, can be precomputed and stored in a look-up table for a given system. Because the solution is symmetric, a small fraction of the entries of W has to actually be computed and stored.

Moreover, we introduced the following highly reliable methods of phase-unwrapping:

(a) Direct phase-unwrapping.

(b) Generalized, iterative phasor method.

Finally, we analyzed and predicted the performance of our newly developed algorithms. Performance predictions are very promising (predicted performance meets and exceeds the goals set by the staff of the Naval Weapons Center (NWC), China Lake, California). Performance curves show that a 5×5 array trying to image an extended target (consisting of 3×3 speckles) at a signal to noise ratio of 0 dB per element per look (with a total of 20 available looks) will only suffer a 1 dB loss in the normalized mainlobe gain of its point spread function after applying our optimal solution. Computer simulations verified this result. To the best of our knowledge, such performance is unprecedented.

0.6 Implications for Further Research

This Phase I SBIR study leads to a Phase II where we propose to build the 10×10 array experimental system described in Section 3.1.2, and use it in order to demonstrate the validity and performance of our advanced self-cohering techniques under realistic conditions. This experimental set-up will allow us to:

(1) Introduce true mechanical errors.

(2) Experiment with different array geometries.

(3) Introduce vibrations within the array. This can simulate an airborne system (above the clouds) for a Theater Missile Defense (TMD) scenario.

(4) Image a target through significant atmospheric turbulence (for possible TMD applications).

(5) Upgrade the working bandwidth of the system by upgrading the data acquisition and data transfer systems.

0.7 Related Reports and Publications

A list of related reports and publications is provided in Section 0.8. Reference [1] is a viewgraph presentation given to **Interspec** technical staff about some of the applications of large-aperture, coherent array lidar in the SDI environment. A description of the experimental system at NWC is also included in [1]. References [2-5] describe the Spatial Correlation Algorithm (SCA) in details. Reference [5] is the notes from a short course given to the research staff of the Naval Weapons Center (NWC) by **Interspec**. The course discussed various self-cohering techniques developed by **Interspec** as well as by other authors. Additional useful material about the subject can be found in references [6-9].

Reference [10] gives a good treatment of the related Knox-Thompson Algorithm, used in astronomy (adaptive optics) in order to achieve diffraction-limited imaging from very large telescopes in the presence of atmospheric turbulence. Similar to the SCA, phase differences are obtained from correlation measurements. On the other hand, optical telescopes are passive sensors responding to <u>incoherent</u> radiation. Incoherence is a major advantage in adaptive optics. A major contribution of the SCA is that it "decoheres" radar returns by range or rotation diversity (or by a combination of both).

References [11,12] are based on the Shear Averaging Algorithm (SAA) of Fienup. In [11], Fienup shows that the SAA is identical to the SCA in its basic form. However, our work preceded the SAA by several years [2,3]. Reference [12] describes applying the SAA to a two-dimensional optical coherent array (with an experimental set-up very similar to that at NWC). In [12], use has been made of results readily available in the optical literature with regard to Knox-Thompson imaging [10]. In this Phase I SBIR effort, we went well beyond these results in the following important respects:

(1) We developed the *optimal* solution to the problem (the weighted least squares solution), for which we derived the input covariance matrix of all phase measurements.

(2) We developed far more reliable phase-unwrapping methods.

(3) We analyzed self-cohering performance in terms of a more tangible criterion (expected loss in the mainlobe of the point spread function) that takes into account all relevant system parameters (as embodied in the input covariance matrix of phase measurements and the transfer matrix of the set of overdetermined equations).

(4) Combined with our phase-unwrapping methods, our optimal solution is <u>direct</u> in the sense that it works on all phase measurements at once. This minimizes the chance

of accumulating errors due to unresolved 2π ambiguities along the way, a serious problem that can arise in the sequential method described in [10] and adopted by [12] (a similar sequential method is also described in [13]).

Reference [14] describes the experimental system at NWC in details. In reference [15], a similar laser radar concept is described. The authors adopt the competing approach of "phase retrieval". However, this approach is known to suffer from serious uniqueness and convergence problems for coherently illuminated objects [16]. Reference [16] reports on successful imaging experiments at NWC based on extending the SCA to two-dimensions in ways similar to [12].

0.8 References

[1] S.E. Clark and L.R. Jones (Naval Weapons Center, China Lake, Cal.), "Electronically Combined Coherent Arrays (ECCA) for Laser Radars," a viewgraph presentation given to **Interspec** technical staff, Ambler, PA, May, 1990.

[2] E.H. Attia, "Phase Synchronizing Large Antenna Arrays Using the Spatial Correlation Properties of Radar Clutter," *National Radio Science Meeting (URSI)*, Boulder, Colorado, January 1984, Meeting Digest p. 105.†

[3] E.H. Attia, Phase Synchronizing Large Antenna Arrays Using The Spatial Correlation Properties of Radar Clutter, Ph. D. Thesis, The Moore School of Electrical Engineering, University of Pennsylvania, 1984.

[4] E.H. Attia and B.D. Steinberg, "Self-Cohering Large Antenna Arrays Using The Spatial Correlation Properties of Radar Clutter," *IEEE Trans. Antennas and Propagation*, Vol. AP-37, No. 1, pp. 30-38, January 1989.

[5] E.H. Attia and K. Abend, *Algorithms for Array Self-Phasing/Self-Cohering*, a short course given to the research staff of Naval Weapons Center, China Lake, CA, March 1991.

[6] K. Abend, E.H. Attia, B. Fell, E. Stockburger, and H. Subbaram, *Synchronizing and Cohering a Distributed Sparse Array Radar*, Phase II Final Report, SBIR No. AF87-173, Contract No. F04701-88-C-0117, prepared by **Interspec**, Inc. for USAF/SD, January, 1991.

[7] B.D. Steinberg and H. Subbaram, *Microwave Imaging Techniques*, John Wiley & Son, New York, 1991.

[8] E.H. Attia, "Self-Cohering Airborne Distributed Arrays Using the Robust Minimum Variance Algorithm," *IEEE AP-S and URSI International Symposium*, Philadelphia, Symposium Digest, Vol. 2, pp. 603-606, June 1986.

[9] E.H. Attia, *Self Cohering Airborne Distributed Arrays*, **Interspec** final report on contract No. F10628-C-0080 for Rome Air Development Center, Hanscom, MA, December 1985.

[10] P. Nisenson, "Speckle Imaging with the PAPA Detector and the Knox-Thompson Algorithm," in *Diffraction-Limited Imaging with Very Large Telescopes*, D.M. Alloin and J.M. Mariotti, eds., Kluwer, Boston, 1989, pp. 157-169.

[11] J.R. Fienup, "Phase Error Correction by Shear Averaging," Signal Recovery and Synthesis III, Topical Meeting, 14-16 June 89, 1989 Technical Digest Series, Vol. 15, *Optical Soc. of Am.*, Washington, DC.

† This paper won the Third Prize in the Student Prize Paper Competition held at the National Radio Science Meeting (URSI), Boulder, Colorado, January 1984.

[12] J. Cederquist, J. Fienup, J. Marron, T. Schultz, and J. Seldin "Digital Shearing Laser Interferometry for Heterodyne Array Phasing," *Proc. SPIE*, Vol. 1416, pp. 266-277, 1991.

[13] H. Takajo and T. Takahashi, "Least Squares Phase Estimation from the Phase Difference," *J. Opt. Soc. Am. A*, Vol. 5, pp. 416-425, March 1988.

[14] S. Clark, L. Jones, and L. DeSandre, "Coherent Array Optical Imaging," *Appl. Opt.*, Vol. 30, pp. 1804-1810, 1991.

[15] P. Henshaw and D. Lee, "Electronically Agile Multiple Aperture Imager Receiver," *Proc. SPIE*, Vol. 828, pp. 134-139, 1987.

[16] S. Clark, L. Jones, and L. DeSandre, "Phasing-up Multiple Aperture Laser Radar Receivers Using Extended Sources," in Technical Digest on Coherent Laser Radar Technology and Applications, *Opt. Soc. Am.*, Vol. 12, pp. 82-84, 1991.

1.0 INTRODUCTION

1.1 Background

Optical sensors fit the strategic defense environment quite naturally. Space-based optical sensors do not suffer from atmospheric attenuation or weather problems that normally limit the utility of ground-based/airborne optics. Compared to radar, optical sensors offer in general reduced weight, size, and power requirements for comparable detection and angular resolution performance. They are also less susceptible to ground-based jammers.

While passive infrared (IR) optical sensors offer large area coverage rates and a specially heightened sensitivity to detecting rocket plumes (especially during the boost phase, which makes them extremely valuable for early warning), they only provide angle-angle measurements. Range and doppler information is lost because of the passive noncoherent nature of IR sensors. Laser radars (lidars) fill this void. In addition to providing the valuable range information, they offer exceptionally high doppler sensitivity and pointing accuracy. The extraordinary doppler sensitivity offered by lidars (combined with high range and angular resolution) is essential to a number of discrimination schemes. A possible active discrimination concept relies on lidar measurements to observe bus kinetic reaction during the deployment of decoys and re-entry vehicles. Because of large mass differences between decoys and re-entry vehicles, the warhead-carrying bus is expected to react differently depending on whether a decoy or a true re-entry vehicle is being ejected. Lidar measurements are also essential to a number of interactive discrimination concepts (using an interactive probe during midcourse). They are also vital for early discrimination during the terminal phase. In addition to the critical role lidars are expected to play in various aspects of the paramount discrimination problem, they are also expected to play indispensable roles in target tracking, pointing, and fire control.

Large aperture laser radars are needed for strategic defense applications. Large apertures are necessary in order to achieve the required detection and angular resolution performance at the long ranges involved. Building a large monolithic transmit/receive optical aperture poses a number of problems. Holding mechanical tolerances (to within a small fraction of the optical wavelength) over such a large aperture will be extremely difficult in the face of orbital temperature changes and mechanical vibrations associated with gross steering of the whole aperture. Other problems include poor beam agility, high power requirements for beamsteering, and launch constraints on the size of the monolithic aperture.

We have proposed a bistatic laser radar system where a relatively small aperture provides the illumination, while a large, thinned, phased array (composed of a number of subapertures) is used on receive. Optical echoes received by the subapertures are to be coherently combined after down-conversion (heterodyning) into baseband electronic signals. Both of

the transmit and receive apertures are envisioned to be mounted on the same platform. Such a sensor, if feasible, offers a number of significant advantages over a large monolithic lidar of comparable detection performance. These advantages include [1]:

(1) High beam agility and reduced power requirements for beamsteering. Multiple simultaneous receive beams can be formed (computed) in the signal processor. The need for physically steering the transmit and receive beams is highly reduced.

(2) Large system "trade space" which for a given performance can lead to a substantial cost and weight saving (e.g., the tradeoff between transmitter and receiver aperture sizes).

(3) Greater light collection for range doppler imagery (RDI). This results in improved signal-to-noise-ratio (SNR) and working range in RDI mode.

(4) Substantially greater angular resolution which can lead to either

  (4.a) Angularly separated imaging (ASI) i.e., the ability to spatially separate targets, or

  (4.b) True angularly resolved imagery (ARI) i.e., "seeing" details on an individual target. This allows up to 4-dimensional (R-D-A-A) imagery and maximizes the information obtainable about the targets.

(5) True bistatic operation (not restricted to round-trip dwell time before repointing).

(6) Sparse arrays offer greater resolution with only a modest increase in weight. Without arrays, long-range space-based laser radars will be quite heavy.

(7) Holding mechanical tolerances over the relatively small transmit aperture and the individual receive subapertures is much easier.

In spite of all of the above favorable features, the problem of coherently combining the outputs of the receive subapertures needs to be solved. Trying to maintain the required mechanical tolerances on the locations of the phase centers of the receive subapertures (in order to achieve acceptable phased array performance) defeats a major purpose of the proposed concept, namely, making large optical apertures possible without requiring strict mechanical rigidity. As mentioned earlier, maintaining the required mechanical tolerances throughout the array will be extremely difficult given the large size of the whole receive aperture. Our approach maintains the required tolerances only within the relatively small subapertures. Meanwhile, the requirements on knowing the locations of the phase centers of these subapertures (within the large array) are significantly relaxed. This way, larger receive apertures will be made possible. Even launch constraints on aperture size could be loosened as folding the array during launch might become possible.

Without accurate knowledge of the locations of the elements of the receive array, our approach depends on compensating for element position errors adaptively (closed-loop).

using returns from the target area. A number of techniques can achieve this goal. We refer to them as "self-cohering" techniques. The simplest of these techniques depends on finding a "phase-up" source within the target area and conjugating its phase across the aperture (in the signal processor). This procedure focuses the array on that source. Only limited knowledge of element positions is needed in order to scan the formed receive beam in angle within the target area (i.e., forming multiple simultaneous receive beams).

It should be noted that the basic approach has been described by other authors [1]. We realized the existence of an ample opportunity for us to significantly contribute to the success of the basic concept in the following ways:

(1) Applying a number of innovative self-cohering techniques to the problem. These advanced techniques (developed by **Interspec**) offer significantly better performance and reliability compared to simple phase conjugation of a phase-up source of opportunity. One technique synthesizes a *superior* phase-up source from *all* potential sources (of *inferior* phasing quality) that might exist in the target area. Another technique utilizes the spatial correlation properties of the reradiated field in order to estimate the required phase corrections.

(2) Offering a unique and deep understanding of self-cohered systems. This expertise encompasses their potential, limitations, and algorithms necessary to their success. Our experience stems from working for about a decade with distorted apertures (real or synthetic) in a radar environment (mostly at microwave frequencies) in order to obtain diffraction-limited performance.

As mentioned above, space-based large aperture laser radars are expected to play an important role in discrimination, target tracking, pointing, and fire control for strategic defense. The same concept could also be applied to the difficult problem of theater missile defense (TMD) using an airborne platform (above the clouds). Our advanced self-cohering techniques significantly enhance the reliability, angular resolution, and detection performance of large aperture coherent optical arrays.

1.2 Study Objectives and Tasks

Phase I of this SBIR was awarded by SDIO (through ONR) with an effective date of June 1, 1991. The main objective was to determine the feasibility of applying our advanced self-cohering techniques to the large-aperture, coherent array lidar problem. Specifically, we had the following objectives:

(1) To adapt a number of our advanced self-cohering techniques to large-aperture coherent array lidar.

(2) To evaluate and quantify the improvements offered by our techniques.

The tasks performed under this effort are:

(1) Baseline Development

(2) Adaptation of Modern Self-Cohering Techniques

(3) Prediction of Expected Performance, and

(4) Design of a Phase II Experiment.

Discussions with Dr. Stuart Clark, Loughborough University, United Kingdom, currently working at US Naval Weapons Center, China Lake, CA, has resulted in a series of recommendations to best use resources under this contract. In a letter from Dr. Louis DeSandare of NWC to Dr. William Miceli of the ONR, it was recommended that Task 1 be de-emphasized and we make use of the results of existing study reports issued by MIT Lincoln Laboratory to establish a set of performance goals. These goals were relayed to us by both Dr. Clark and Dr. DeSandre.

Task 2 has focused on extending the Spatial Correlation Algorithm (SCA), [2,3], to two-dimensional array geometries. We realized that the SCA is the most promising of all existing self-cohering techniques because of its ability to correct arbitrarily large phase errors that can be totally independent from array element to another. Another reason that made us exclude other algorithms such as the Multiple Scatterer Algorithm (MSA), [4-7], was that we were able to show that the SCA itself can work as a superior "multiple scatterer algorithm" for the case where we have a limited number of looks with some of which containing dominant scatterers. Correlation measurements based exclusively on these special looks (processed according to the SCA) proved to be a better way of achieving effective self-cohering [6].

1.3 Summary of Important Results

The main result of this Phase I SBIR study is that "self-phasing" of a large receive array of optical subaprtures is quite feasible using our advanced "self-cohering" techniques. That is, it is possible, for a bistatic laser radar system, to obtain diffraction-limited performance from a badly distorted, large, optical receive aperture adaptively (using returns from the target area). No strong point source is required. Instead, a number of independent "looks" from the target are needed. These looks can be obtained via either of the following two methods (or by a combination of both):

(1) By range diversity. That is, if the laser radar can resolve the target into a number of range cells, then each target range cell will provide us with an independent look.

(2) By rotation diversity. A rotating target with a diffuse surface will provide us with a number of independent looks as we observe it over time. Because of the short optical wavelengths involved, a small rotation from pulse to pulse is sufficient to decorrelate the looks.

During the course of this study, we developed a number of advanced self-cohering techniques suited to the problem. In particular, we developed:

(1) Least squares two-dimensional (2-D) SCA.

(2) Weighted least squares (minimum variance) 2-D SCA.

(3) The SCA as a "multiple scatterer algorithm".

The first two techniques can be considered as extensions of the Spatial Correlation Algorithm (SCA) to two-dimensional array geometries. The second algorithm provides the optimal solution to the problem given a reasonable number of looks. For the case where we have a limited number of looks and some of which contain dominant scatterers, the third technique exploits these special looks in order to achieve effective self-cohering.

All three techniques solve a set of overdetermined equations relating array distortion to phase measurements. The solutions take on the general form

$$\underline{\delta} = W\underline{\Psi}, \tag{1.1}$$

where $\underline{\delta}$ is the vector of phase corrections, W is a weighting matrix, and $\underline{\Psi}$ is the vector of differential phase measurements.

We developed a symmetric phase constraint that resulted in a symmetric solution amenable to fast matrix inversion algorithms (needed for computing W). Notice that the optimal weights, W, can be precomputed and stored in a look-up table for a given system. Because the solution is symmetric, a small fraction of the entries of W has to actually be computed and stored.

Phase-unwrapping of $\underline{\Psi}$ is essential before applying (1.1). We developed the following methods of phase-unwrapping:

(a) Direct phase-unwrapping.

(b) Generalized, iterative phasor method.

Both methods, (a) and (b), require an initial solution for array phase corrections. We developed two techniques for obtaining such an initial solution (see Section 2.3.4):

(i) Direct integration of phase differences starting from an element near array center and moving outwards (radially) in all directions (quickest method).

(ii) Sequential near-optimal/optimal solutions for subarrays of growing size (most reliable method).

We analyzed and predicted the performance of our newly developed algorithms. Performance predictions are very promising (predicted performance meets and exceeds the goals set by the staff of the Naval Weapons Center (NWC). China Lake, California). Performance curves show that a 5×5 array trying to image an extended target (consisting of 3×3 speckles) at a signal to noise ratio of 0 dB per element per look (with a total of 20 available looks) will only suffer a 1 dB loss in the normalized mainlobe gain of its point spread function after applying our optimal solution. Computer simulations verified this result. To the best of our knowledge, such performance is unprecedented.

In general, extensive computer simulations have verified all our algorithms and performance predictions.

We have also designed two sets of Phase II experiments for the purpose of demonstrating our advanced self-cohering techniques:

(1) Using the NWC experimental system:

(1.1) A number of useful experiments can be performed with existing hardware.

(1.2) On the other hand, the existing CCD array has a very low bandwidth and offers no significant geometrical flexibility.

(2) Building a 10×10 array of individual detectors. This approach makes it possible to test our techniques under realistic conditions. Such an experimental set-up will enable us to:

(1) Introduce true mechanical errors.

(2) Experiment with different array geometries.

(3) Introduce vibrations within the array. This can simulate an airborne system (above the clouds) for a Theater Missile Defense (TMD) scenario.

(4) Image a target through significant atmospheric turbulence (for possible TMD applications).

(5) Upgrade the working bandwidth of the system by upgrading the data acquisition and data transfer systems.

1.4 References

[1] S.E. Clark and L.R. Jones (Naval Weapons Center, China Lake, Cal.), "Electronically Combined Coherent Arrays (ECCA) for Laser Radars," a viewgraph presentation given to **Interspec** technical staff, Ambler, PA, May, 1990.

[2] E.H. Attia and B.D. Steinberg, "Self-Cohering Large Antenna Arrays Using The Spatial Correlation Properties of Radar Clutter," *IEEE Trans. Antennas and Propagation*, Vol. AP-37, No. 1, pp. 30-38, January 1989.

[3] E.H. Attia, Phase Synchronizing Large Antenna Arrays Using The Spatial Correlation Properties of Radar Clutter, Ph. D. Thesis, The Moore School of Electrical Engineering, University of Pennsylvania, 1984.

[4] E.H. Attia, "Self-Cohering Airborne Distributed Arrays Using the Robust Minimum Variance Algorithm," *IEEE AP-S and URSI International Symposium*, Philadelphia, Symposium Digest, Vol. 2, pp. 603-606, June 1986.

[5] E.H. Attia, *Self Cohering Airborne Distributed Arrays*, **Interspec** final report on contract No. F10628-C-0080 for Rome Air Development Center, Hanscom, MA, December 1985.

[6] E.H. Attia and K. Abend, *Algorithms for Array Self-Phasing/Self-Cohering*, a short course given to the research staff of Naval Weapons Center, China Lake, CA, March 1991.

[7] B. Kang, H. Subbarram (Interspec), and B.D. Steinberg, "Improved Adaptive-Beamforming Target for Self-Calibrating a Distorted Phased Array," *IEEE Trans. Antennas and Propagation*, Vol. AP-38, No. 2, pp. 186-194, February 1990.

2.0 TWO-DIMENSIONAL SELF-COHERING

2.1 Introduction

As mentioned earlier, most of our algorithmic work during this effort has focused on extending the Spatial Correlation Algorithm (SCA) [1-3] to two-dimensional array geometries. We realized that the SCA is the most promising of all existing self-cohering techniques because of its ability to correct arbitrarily large phase errors that can be totally independent from one array element to another without requiring a phase-up source. Moreover, the SCA proved to work as a superior "multiple scatterer algorithm" in situations where we have a limited number of looks with some of which containing dominant scatterers. Correlation measurements based exclusively on these special looks (processed according to the SCA) proved to be a better way of achieving effective self-cohering.

Although, the SCA has been developed for the purpose of phase cohering a distorted array in the absence of a strong point source (a dominant scatterer or a beacon) using the spatial correlation properties of radar clutter, the algorithm was shown to work exceptionally well using returns from man-made targets. The SCA reliably predicts and corrects aperture distortion. Array distortion can be geometrical (due to lack of accurate knowledge of element positions resulting, for example, from airframe vibrations), or optical/electrical (due to different lengths of the optical fibers distributing the LO signal to coherent detectors, mismatches, etc.). Moreover, distortion of the phase front due to propagation anomalies can often be modeled as a pattern of phase errors across the array and hence can be compensated for. The array itself is assumed to be fairly general. It can be random or periodic, physical or synthetic, one- or two-dimensional, transmit/receive or receive only. The main restriction is that the **interelement** spacing should not exceed the spatial correlation distance of the reradiated field. For a man-made target, this distance is roughly equal to $\frac{\lambda}{2L}R$, where λ is the wavelength, L is target size, and R is range. This distance can be much greater than $\lambda/2$, allowing the receive array to be highly thinned. Moreover, we can show that the restriction on inerelement spacing can be significantly relaxed, by doppler processing of target returns [4], whenever a net rotation exists in the relative motion between the target and lidar platform.

In this section, we extend the spatial correlation algorithm to two-dimensional array geometries. However, for reasons of continuity, we first introduce the original one-dimensional SCA.

2.2 One-Dimensional SCA

The SCA relies, in its simplest forms, on measuring the nearest-neighbor spatial correlation between target signals received by the array elements over range. The basic idea behind the algorithm is that $R(X)$, the spatial correlation function of target returns at the receive aperture will be **real** provided that scatterers (illuminated by the mainbeam of the transmitter) are statistically homogeneous when averaged over a number of independent looks. Nonzero arguments of the measured correlations are attributed to phase errors at the array. We will show that array phase errors can be estimated from the correlation measurements and hence can be compensated for.

To illustrate, let us consider the simple case of a linear, periodic, receive array with interelement spacing d. Let us also assume that the transmit and receive apertures are cocentered and the transmit beam is steered to the broadside direction of the receive array. In the absence of any phase errors in the array, each pair of adjacent elements (forming an interferometer of size d) should measure the **same** quantity $R(d)$ irrespective of its position along the array. This is a direct consequence of the assumed spatial stationarity of the random process representing target returns across the receive aperture as observed over a number of independent looks. Further, if $R(d)$ is real, then each element pair will be measuring $|R(d)|e^{j0}$. However, in the presence of a phase error pattern $\{\delta_n \,|\, n = 1, \cdots, N\}$ across the N-element array, correlation measurements will start to reflect these phase errors. In particular, the $n\,\underline{th}$ correlator (formed by elements number n and $n+1$) will be measuring $|R(d)|e^{j[\delta_n - \delta_{n+1}]}$. That is, the argument of the correlation measurement made by any such element pair gives a direct estimate of the difference between the two phase errors suffered by the pair of elements involved. We will show that the available $N-1$ such phase difference estimates are sufficient to estimate the phase error pattern across the receive aperture (within an unknown but unimportant additive constant phase term). The estimated phase error pattern can now be used to cohere the array by subtracting it from the phases of the received data across the aperture off-line. Then, multiple simultaneous beams can be formed by Fourier transforming the corrected data. It is important to notice that the SCA places no restrictions on the range of initial phase errors it can correct for. Since the solution is direct (non-iterative), initial phase errors can range anywhere between $-\pi$, $+\pi$ without affecting the performance of the algorithm.

Let us assume that the field measured at the $n\,\underline{th}$ element is given by $e'_n = e_n e^{j\delta_n}$ where e_n is the error-free value produced by a large number of non-coherent scatterers on the surface of the illuminated target, and δ_n is the phase error due to array distortion. The $n\,\underline{th}$ correlator provides an estimate, $\hat{R}'_n$ of the quantity

$$\begin{aligned} R'_n &= E\{e'_n e'^{*}_{n+1}\} = E\{e_n e^{*}_{n+1}\} e^{j(\delta_n - \delta_{n+1})} \\ &= R(d) e^{j(\delta_n - \delta_{n+1})} \,. \end{aligned}$$

R'_n is estimated over a number of independent looks. If we have M looks, we compute

$$\hat{R}'_n = \frac{1}{M} \sum_{i=1}^{M} e'_{i,n} e'^{*}_{i,n+1} ,$$

where i denotes the $i\,\underline{th}$ look.

The phase of $\hat{R}'_n$, called ψ_n, is the quantity of interest. Assuming that we have good phase estimates $\{\psi_n\}$, we can approximately write

$$\psi_n \approx (\delta_n - \delta_{n+1}) + \beta \qquad n = 1, \ldots, N-1 \tag{2.1}$$

where $\beta = \arg\{R(d)\}$.

Now we form the quantity

$$o_n \equiv \sum_{k=1}^{n-1} \psi_k \tag{2.2}$$

$$\approx (\delta_1 - \delta_n) + (n-1)\beta \tag{2.3}$$

which we use as a phase correction by adding it at the $n\,\underline{th}$ element (for all n). The total phase shift becomes

$$\delta\phi_n = \delta_n + \phi_n \tag{2.4}$$

$$\approx \delta_1 + (n-1)\beta \tag{2.5}$$

Now the phase $\beta(X)$ of the spatial correlation function plays a major role in cohering the array. If the spatial correlation function is real and positive in the region of interest ($\beta = 0$), we have an ideal situation, for then (2.5) reduces to

$$\delta\phi_n \approx \delta_1 = \textit{constant independent of } n \tag{2.6}$$

and the random variable δ_n has been replaced by a constant. The result is a well-formed beam pointing roughly at target cenroid. It is straightforward to see that the same result applies to ***nonperiodic*** arrays as long as $R(X)$ is real.

Let us for the moment assume a search scenario where most radar returns are due to ground or sea clutter. The assumption that the spatial correlation function at the aperture, $R(X)$, should be real is a direct consequence of the Fourier transform relationship that exists between the clutter illumination intensity function, $I(u)$, and $R(X)$ [1-3]. Here, $u = \sin\theta$ where θ is the angle measured off the axis of the illuminator, and X is measured along the receive aperture. $I(u)$ describes the average power reradiated by the scattering centers within the illuminated sector as a function of the reduced angular variable u. If clutter is statistically homogeneous over range, $I(u)$ will be proportional to $|f(u)|^2$, the power

pattern of the transmitter which is real by definition. A real symmetric $I(u)$ will result in a real $R(X)$. For example, the radiation pattern of a uniform aperture will be proportional to $\text{sinc}Du/\lambda$ and $I(u)$ will be proportional to $\text{sinc}^2 Du/\lambda$. The autocorrelation function $R(X)$, being the Fourier transform of $I(u)$, will be triangular with base $2D$. In general, the correlation distance will be on the order of D. Thus, the largest interelement distance in the receiving array should not exceed D (with some margin).† It is worthwhile to note that the Fourier transform relationship that exists between $R(X)$ and $I(u)$ in the space-angle domains is very similar to the Wiener-Khinchine theorem that relates the temporal autocorrelation function $R(\tau)$ and the power spectral density $S(f)$ of a temporal random process in the time-frequency domains.

The independent looks needed for estimating the required correlations can be obtained via either of the following two methods (or by a combination of both):

(1) By range diversity. That is, if the laser radar can resolve the target into a number of range cells, then each target range cell will provide us with an independent look.

(2) By rotation diversity. A rotating target with a diffuse surface will provide us with a number of independent looks as we observe it over time. Because of the short optical wavelengths involved, a minute rotation from pulse to pulse is sufficient to decorrelate the looks.

It should be noted that the spatial correlation algorithm is a very robust self-cohering technique. Although independence of the target scene can be forced by estimating the correlation values over a large number of looks (using fine range resolution and or exploiting target rotation) to insure statistical homogeneity of scatterers, the algorithm will not fall apart easily if this condition becomes increasingly unsatisfied. Even if $R(X)$ were complex ($\beta \neq 0$), it would still be possible to self-cohere a *periodic* aperture. A small beam pointing error proportional to the slope of the phase of $R(X)$ will result in this case however. This can easily be seen from (2.5) where the linear phase term $(n-1)\beta$ will cause the image shift. Moreover, it can be shown that even if the array were *nonperiodic* and $R(X)$ is complex but has a linear phase, it would still be possible to self-cohere the aperture. A beam pointing error proportional to the slope of the phase of $R(X)$ will result in this case too. The condition of phase linearity of $R(X)$ will also be valid (to first order) for a general scene because the argument of $R(X)$ has to be an odd function all the time because $I(u)$, the Fourier transform of $R(X)$, is always real (by definition).

As mentioned earlier, experimental evidence has shown that the SCA works remarkably well when applied to returns from man-made extended targets such as aircraft [6]. A surprisingly small number of range bins was needed in order to achieve effective self-cohering. These results are attributed to the above-mentioned inherent resiliency of the

† For a man-made target, this distance is roughly equal to $\frac{\lambda}{2L}R$, where λ is the wavelength, L is target size, and R is range.

algorithm. Moreover, as mentioned earlier, the SCA proved to work as a superior "multiple scatterer algorithm" in situations where we have a limited number of looks where some of which are dominated by specular reflections. Correlation measurements based exclusively on these special looks (processed according to the SCA) proved to be a better way of cohering the array.

Notice that a number of generalizations are straightforward:

(1) The transmit beam does not have to be steered to the broadside direction. For targets at other angles, using the same processing described above, the formed receive beam will be retrodirective; it will always follow target centroid. This is because correlation measurements in this case will show the difference in phase due to angle of arrival in addition to the difference in array phase errors. Estimating the sum of the angle of arrival linear phase term plus the phase error term at each element and subtracting the sum from the phases of the received data across the array forms a "retrodirective" receive beam in the sense that direct summation of the corrected data will form a beam in the direction of the center of the illuminated target.

(2) The array does not have to be periodic. For a linear, nonperiodic (or random) array, the correlators will be measuring $|R(x_i - x_{i+1})|e^{j[\delta_i - \delta_{i+1}]}$ as long as $R(X)$ is real. The argument of the correlation measurement (which is what we process) will remain unchanged provided that the interelement distance $(x_i - x_{i+1})$ does not exceed the spatial correlation distance.

(3) Nearest-neighbor correlations provide the minimum amount of information needed to estimate the phase error pattern (and hence cohere the array). Following the nomenclature used for periodic arrays (or periodically sampled time-domain data), we will refer to nearest-neighbor correlations as "first-lag" correlations. With this nomenclature, the correlation between elements number i and $i+2$ will be referred to as a "second-lag" correlation and so on. For the case where the maximum first-neighbor interelement distance is much smaller than the spatial correlation distance of target returns, "multiple-lag" correlations can be used to set a number of over-determined equations that can be solved for the receive phase errors in the least square error sense to improve the performance of the algorithm [1,2,5,6].

(4) The array does not have to be linear. The algorithm can be extended to treat two-dimensional arrays. Two-dimensional geometries are inherently over-determined in the sense that there are more equations (or measurements) than there are unknowns. Single-lag as well as multiple-lag equations can be set to estimate the 2-D phase error pattern across the receive array.

(5) The transmit and receive apertures do not have to be exactly cocentered. The algorithm will be tolerant to considerable displacements in the centers of the two

apertures provided that the bistatic angle (from the transmitter to the target area and back to the receiver) is small. The formed receive beam will still be pointing at the center of the illuminated target.

2.3 Extending the SCA to Two Dimensions

For a one-dimensional receive array using only nearest-neighbor correlation phase measurements, the number of equations (differential phase errors) equals the number of unknowns (phase corrections) and hence a unique solution exists. For a two-dimensional array, the problem is inherently over-determined in the sense that there are more equations (or measurements) than there are unknowns. Figure 2.1 illustrates the situation for an $N \times M$ periodic array. Here, the number of unknowns is

$$N_u = NM - 1 \tag{2.7}$$

If we consider first-neighbor correlations only (Case 1, Figure 2.1.a), the number of equation (which is equal to the solid lines connecting element pairs) is given by

$$N_e = 2NM - (N + M)\,, \tag{2.8}$$

which is roughly equal to twice the number of unknowns for large arrays ($N, M \gg 1$).

If we consider diagonal neighbors as well (Case 2, Figure 2.1.b), the number of equations becomes

$$N_e = 4NM - 3(N + M) + 2\,, \tag{2.9}$$

which is roughly equal to four times the number of unknowns for large arrays.

Keeping the same notation of the previous section, and assuming a real two-dimensional spatial correlation function $R(X, Y)$, our over-determined set of equations will have the general form

$$\delta_{ij} - \delta_{kl} \approx \psi_{ij,kl}\,, \tag{2.10}$$

where δ_{ij} is the needed phase correction (unknown) for the array element at location (i, j) of a rectangular grid as shown in Figure 2.2. Similarly, $\psi_{ij,kl}$ is the phase of the correlation measured between the two elements at locations (i, j) and (k, l). Notice that the implicit assumption of a periodic array is not necessary. We only make it here for the sake of simplicity.

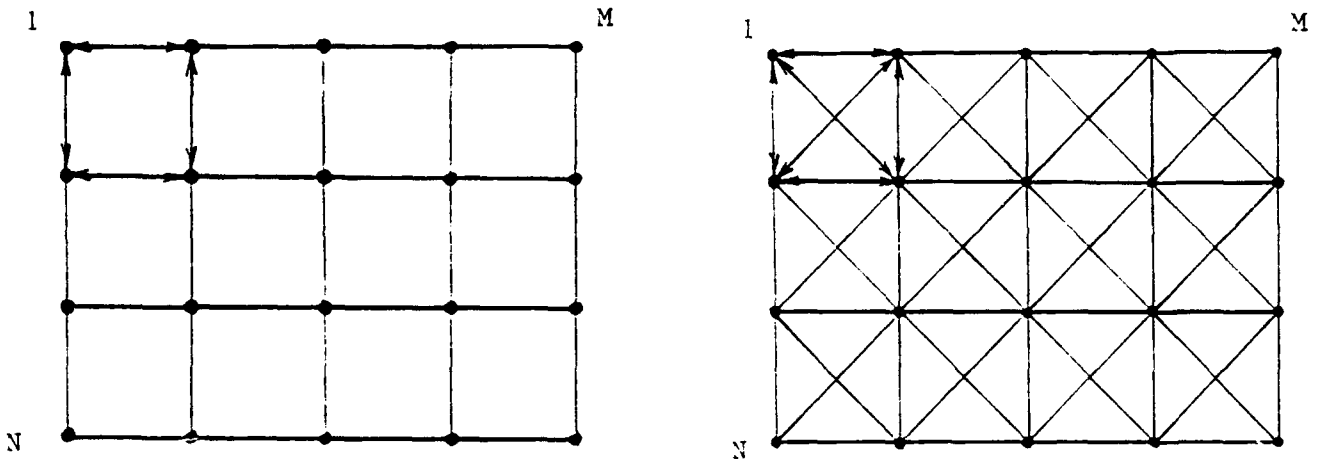

(a) (b)

Figure 2.1. Two possible sets of phase measurements for an $N \times M$ periodic array are shown. In Case 1. (a), only first-neighbor correlations are considered. In Case 2. (b), diagonal neighbors are considered as well.

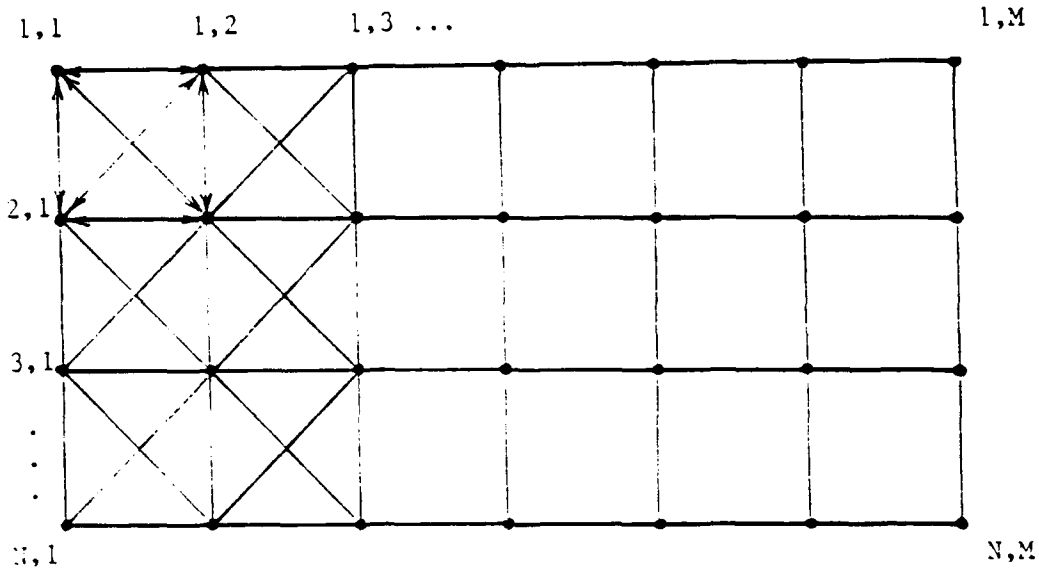

Figure 2.2. A two-dimensional rectangular grid.

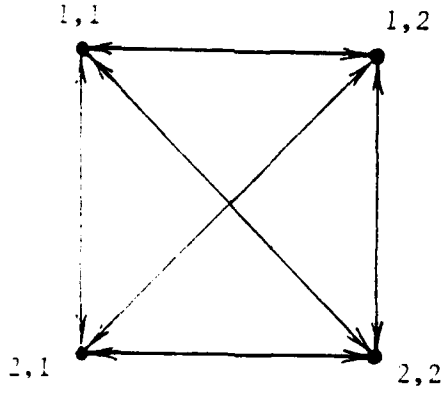

Figure 2.3. A 2×2 array.

To illustrate, let us consider the 2 × 2 array shown in Figure 2.3. Here, our equations become

$$\begin{aligned}
\delta_{11} - \delta_{12} &= \psi_{11,12} \\
\delta_{11} - \delta_{21} &= \psi_{11,21} \\
\delta_{11} - \delta_{22} &= \psi_{11,22} \\
\delta_{12} - \delta_{21} &= \psi_{12,21} \\
\delta_{12} - \delta_{22} &= \psi_{12,22} \\
\delta_{21} - \delta_{22} &= \psi_{21,22}
\end{aligned} \tag{2.11}$$

Notice that we dropped the ≈ sign for simplicity. However, the above set of equations, (2.11), is exact provided that we interpret $\{\delta_{ij}\}$ as *estimates* of the true phase errors (which is naturally our intention).

As we did before, one unknown phase quantity could arbitrarily be set to zero. Therefore, we can write

$$\delta_{11} = 0\,, \tag{2.12}$$

which makes the element at $(1,1)$ our phase reference. In matrix form, (2.11) and (2.12) can be written as

$$A\underline{\delta} = \underline{\Psi}\,, \tag{2.13}$$

where,

$$A = \begin{pmatrix} -1 & 0 & 0 \\ 0 & -1 & 0 \\ 0 & 0 & -1 \\ 1 & -1 & 0 \\ 1 & 0 & -1 \\ 0 & 1 & -1 \end{pmatrix}, \tag{2.14}$$

$$\underline{\delta} = \begin{pmatrix} \delta_{12} \\ \delta_{21} \\ \delta_{22} \end{pmatrix}, \tag{2.15}$$

$$\underline{\Psi} = \begin{pmatrix} \psi_{11,12} \\ \psi_{11,21} \\ \psi_{11,22} \\ \psi_{12,21} \\ \psi_{12,22} \\ \psi_{21,22} \end{pmatrix}. \tag{2.16}$$

2.3.1 Least Squares Solution

Let us, for now, make the gross simplifying assumption that the random components of all measurements, $\{\psi_{ij,kl}\}$, are independent and identically distributed random variables, we can solve (2.13) in the least squares error sense [7] and obtain

$$\underline{\delta}_{\text{ls}} = (A^T A)^{-1} A^T \underline{\Psi}\,, \tag{2.17}$$

which, for our 2×2 example, yields

$$\underline{\delta}_{\text{ls}} = \frac{1}{2} \begin{pmatrix} -1 & \frac{1}{2} & 0 & -\frac{1}{2} & -\frac{1}{2} & \frac{1}{2} \\ -\frac{1}{2} & 0 & \frac{1}{2} & -1 & -\frac{1}{2} & -\frac{1}{2} \\ -\frac{1}{2} & -\frac{1}{2} & -\frac{1}{2} & -\frac{1}{2} & -1 & 0 \end{pmatrix} \underline{\Psi}\,. \tag{2.18}$$

2.3.2 A Symmetric Phase Constraint

Examining (2.18), we can readily see that the solution is *asymmetric*. Although all elements of the 2×2 array occupy similar positions with respect to the array (Figure 2.3), the solution combines the measurements differently from one element to another (compare the answer for elements $(1,2)$ and $(2,2)$, for example). The resulting asymmetry is counter intuitive and, as we will show later, has unfavorable computational consequences. We traced the source of the problem to equation (2.12), where we force one element to become our phase reference. Instead of taking $\delta_{11} = 0$, we choose

$$\sum_{i=1}^{N}\sum_{j=1}^{M} \delta_{ij} = 0\,. \tag{2.19}$$

The above phase constraint, (2.19), treats all of the unknowns, $\{\delta_{ij}\}$ equally. It implicitly assumes that all unknown phase quantities are measured with respect to a common phase reference ϕ_o given by

$$\phi_o = \frac{1}{NM} \sum_{i=1}^{N}\sum_{j=1}^{M} \delta_{ij}\,. \tag{2.20}$$

Combining (2.10) and (2.19), we get (after dropping the $\approx$ sign as before)

$$A\underline{\delta} = \underline{\Psi}\,, \tag{2.21}$$

where, for a 2×2 array, we have this time

$$A = \begin{pmatrix} 1 & -1 & 0 & 0 \\ 1 & 0 & -1 & 0 \\ 1 & 0 & 0 & -1 \\ 0 & 1 & -1 & 0 \\ 0 & 1 & 0 & -1 \\ 0 & 0 & 1 & -1 \\ 1 & 1 & 1 & 1 \end{pmatrix}, \tag{2.22}$$

$$\underline{\delta} = \begin{pmatrix} \delta_{11} \\ \delta_{12} \\ \delta_{21} \\ \delta_{22} \end{pmatrix}, \tag{2.23}$$

$$\underline{\Psi} = \begin{pmatrix} \psi_{11,12} \\ \psi_{11,21} \\ \psi_{11,22} \\ \psi_{12,21} \\ \psi_{12,22} \\ \psi_{21,22} \\ 0 \end{pmatrix}. \tag{2.24}$$

Therefore, the least squares solution becomes

$$\underline{\delta}_{\text{ls}} = (A^T A)^{-1} A^T \underline{\Psi} = (4I)^{-1} A^T \underline{\Psi} = \frac{1}{4} A^T \underline{\Psi}. \tag{2.25}$$

where I is the identity matrix. Explicitly, we rewrite (2.25) as

$$\underline{\delta}_{\text{ls}} = \frac{1}{4} \begin{pmatrix} 1 & 1 & 1 & 0 & 0 & 0 & 1 \\ -1 & 0 & 0 & 1 & 1 & 0 & 1 \\ 0 & -1 & 0 & -1 & 0 & 1 & 1 \\ 0 & 0 & -1 & 0 & -1 & -1 & 1 \end{pmatrix} \underline{\Psi}. \tag{2.26}$$

It is straightforward to see that (2.26) is a symmetric solution. The answer for each element combines the measurements in a similar way reflecting the symmetry of the original 2×2 array.

It is important to note that the matrix G defined as

$$G = A^T A \tag{2.27}$$

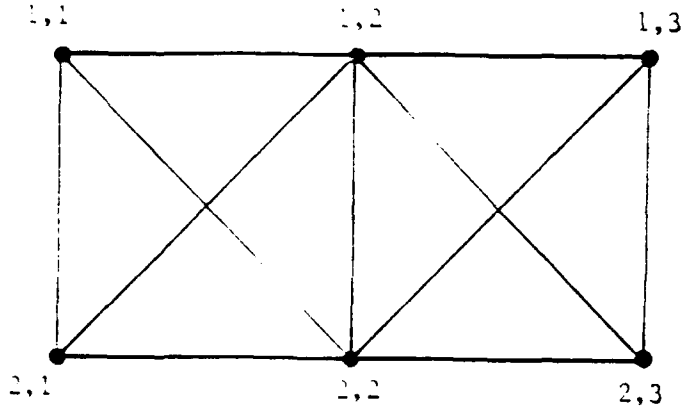

Figure 2.4. A 2 × 3 array.

is not always proportional to I for a general $N \times M$ array. For example, for the 2×3 array of Figure 2.4, we have

$$G = \begin{pmatrix} 4 & 0 & 1 & 0 & 0 & 1 \\ 0 & 6 & 0 & 0 & 0 & 0 \\ 1 & 0 & 4 & 1 & 0 & 0 \\ 0 & 0 & 1 & 4 & 0 & 1 \\ 0 & 0 & 0 & 0 & 6 & 0 \\ 1 & 0 & 0 & 1 & 0 & 4 \end{pmatrix} . \tag{2.28}$$

For a general $N \times M$ array, we can show that G will always be

(1) symmetric and positive definite,

(2) persymmetric (symmetric about the cross diagonal),

(3) sparse,

(4) off-diagonal non-zero entries = 1.

The above properties are a direct consequence of our symmetric phase constraint, (2.19), and can be exploited to efficiently compute G^{-1} [8]. However, further research is needed in order to develop a fast matrix inversion algorithm that utilizes the above properties to their fullest extent. Nevertheless, the symmetry of the answer allows us, as we show below, to develop fast, near-optimal solutions for a general $N \times M$ array.

2.3.3 Weighted Least Squares Solution

As mentioned above, the least squares solution, (2.17), ignores the important fact that correlation measurements taken throughout the array are correlated and exhibit different variances. For example, it is shown in [1,2,6] that the variance of the phase of a correlation measurement grows rapidly as the distance between the two elements involved is increased beyond the spatial correlation distance. More specifically, it is shown in [6] (and in Section 2.3.4) that the variance of these phase estimates is given by

$$\sigma_\psi^2 \approx \frac{1}{2M} \left[\left(\frac{R(0,0) + \sigma_n^2}{R(X,Y)} \right)^2 - 1 \right] , \tag{2.29}$$

where M is the number of looks used in estimating the interelement correlations, and σ_n^2 is the noise power at each element. Here $R(0,0)$ and $R(X,Y)$ are the values of the theoretical spatial correlation function at the origin and at a two-dimensional spatial lag (X,Y) respectively. Notice that $R(X,Y)$ can be computed from the transmitter power pattern and geometry as described previously. The above expression clearly shows that σ_ψ^2

quickly increases as $R(X,Y)$ decreases relative to $R(0,0)$ due to an increasing 2-D spatial lag (X,Y) (especially if $\sigma_n^2 \ll R(0,0)$).

The weighted least-squares solution [7] (which is also known as the "minimum variance solution") provides the optimal estimates of the phase corrections and is given by

$$\underline{\delta}_{\mathbf{mv}} = (A^T \mathcal{R}_I{}^{-1} A)^{-1} A^T \mathcal{R}_I{}^{-1} \underline{\Psi}, \tag{2.31}$$

where $\mathcal{R}_I$ is the covariance matrix of all input phase measurements (notice that if the random components of all phase measurements are independent and identically distributed random variables with a common variance σ^2, then $\mathcal{R}_I = \sigma^2 I$, and (2.31) reduces to (2.17), i.e., $\underline{\delta}_{\mathbf{mv}} = \underline{\delta}_{\mathbf{ls}}$).

It should be noted that $\mathcal{R}_I$ is an $N_e \times N_e$ matrix where the total number of equations, N_e, is revised for Case 2, Figure 2.1.b, from (2.9) to

$$N_e = 4NM - 3(N+M) + 3,$$

to account for the additional equation representing our symmetric phase constraint (2.19). Equation (2.19) gives rise to a mathematical difficulty. As is, the last row and column of $\mathcal{R}_I$ will both consist of zeroes, making $\mathcal{R}_I$ singular. We avoided this difficulty by conceptually writing

$$\sum_{i=1}^{N}\sum_{j=1}^{M} \delta_{ij} = \epsilon \tag{2.32}$$

where ϵ is a fictitious, independent random variable whose variance, σ_ϵ^2, can be made arbitrarily small. This makes the last diagonal entry of $\mathcal{R}_I$,

$$\mathcal{R}_I(N_e, N_e) = \sigma_\epsilon^2, \tag{2.33}$$

making $\mathcal{R}_I$ nonsingular. To our satisfaction, we found that the net result is independent of the value of σ_ϵ^2 (as long as $\sigma_\epsilon^2 > 0$). Therefore, we took

$$\sigma_\epsilon^2 = 1 \tag{2.34}$$

in most of our computations of $\mathcal{R}_I$.

2.3.3.1 Deriving The Error Covariance Matrix

The error covariance matrix, $\mathcal{R}_I$, is defined [7] as

$$\mathcal{R}_I = E\left\{\delta\underline{\Psi}\delta\underline{\Psi}^T\right\}, \tag{2.35}$$

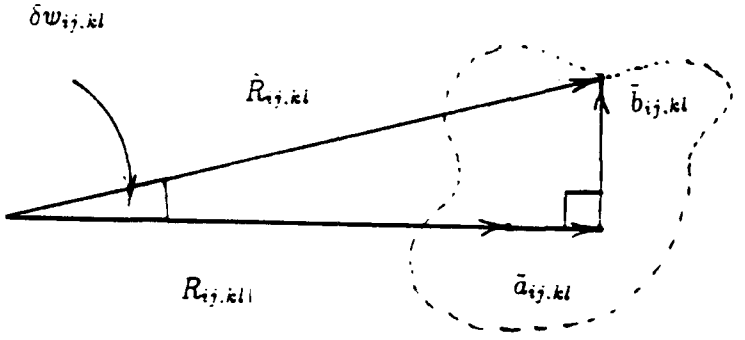

Figure 2.5. A phasor diagram representing phase measurement errors.

where $\delta\underline{\Psi}$ contains the random components of $\underline{\Psi}$, and E denotes expectation. The random component, $\delta\psi_{ij,kl}$, of the phase measurement $\psi_{ij,kl}$ can be shown [1,2] to follow the phasor diagram of Figure 2.5, where $R_{ij,kl}$ stands for $R(x_{ij}-x_{kl}, y_{ij}-y_{kl})$. It is straightforward to show that $E\left\{\hat{R}_{ij,kl}\right\} = R_{ij,kl}$, where

$$\begin{aligned}\hat{R}_{ij,kl} &= \frac{1}{M}\sum_{m=1}^{M}[e_{m,ij}+n_{m,ij}][e_{m,kl}+n_{m,kl}]^* \\ &= (|R_{ij,kl}|+\tilde{a}_{ij,kl}) + j\,\tilde{b}_{ij,kl}\,. \end{aligned} \tag{2.36}$$

As before, M is the total number of independent looks used. $e_{m,ij}$, $n_{m,ij}$ are, respectively, the signal and noise at the receiver output of the array element at location (i,j) due to the m $\underline{th}$ look in the absence of array distortion. Notice that $e_{m,ij}$ is the signal that would be received had broadside illumination been used.

Assuming that the rms value of $\delta\psi_{ij,kl}$ is somewhat small, we can write (see Figure 2.5)

$$\delta\psi_{ij,kl} \approx \frac{\tilde{b}_{ij,kl}}{|R_{ij,kl}|}\,. \tag{2.37}$$

Therefore, entries of $\mathcal{R}_{\mathcal{I}}$ will have the general form

$$\overline{\delta\psi_{ij,kl}\,\delta\psi_{op,qr}} = \frac{\overline{\tilde{b}_{ij,kl}\,\tilde{b}_{op,qr}}}{R_{ij,kl}\,R_{op,qr}}\,, \tag{2.38}$$

where the overbar denotes expectation and we assumed that $R(X,Y)$ is real.

From (2.36), we can write

$$\begin{aligned}\tilde{b}_{ij,kl} = \frac{1}{M}\sum_{m=1}^{M} & e_{s_{m,ij}}e_{c_{m,kl}} - e_{c_{m,ij}}e_{s_{m,kl}} + n_{s_{m,ij}}e_{c_{m,kl}} - n_{c_{m,ij}}e_{s_{m,kl}} + \\ & e_{s_{m,ij}}n_{c_{m,kl}} - e_{c_{m,ij}}n_{s_{m,kl}} + n_{s_{m,ij}}n_{c_{m,kl}} - n_{c_{m,ij}}n_{s_{m,kl}}\,,\end{aligned} \tag{2.39}$$

where

$$e_{m,ij} = e_{c_{m,ij}} + j e_{s_{m,ij}}\,, \tag{2.40}$$

and

$$n_{m,ij} = n_{c_{m,ij}} + j n_{s_{m,ij}}\,. \tag{2.41}$$

Assuming that $e_{m,ij}$ and $e_{n,ij}$ are uncorrelated for $n \neq m$ (looks are assumed to be independent), we get

$$\overline{\tilde{b}_{ij,kl}\,\tilde{b}_{op,qr}} = \frac{1}{M^2}\sum_{m=1}^{M}\overline{e_{s_{m,ij}}e_{c_{m,kl}}e_{s_{m,op}}e_{c_{m,qr}}} - \overline{e_{s_{m,ij}}e_{c_{m,kl}}e_{c_{m,op}}e_{s_{m,qr}}} -$$

$$\overline{e_{c_{m,ij}} e_{s_{m,kl}} e_{s_{m,op}} e_{c_{m,qr}}} + \overline{e_{c_{m,ij}} e_{s_{m,kl}} e_{c_{m,op}} e_{s_{m,qr}}} +$$
$$\overline{n_{s_{m,ij}} e_{c_{m,kl}} n_{s_{m,op}} e_{c_{m,qr}}} - \overline{n_{s_{m,ij}} e_{c_{m,kl}} e_{c_{m,op}} n_{s_{m,qr}}} +$$
$$\overline{n_{c_{m,ij}} e_{s_{m,kl}} n_{c_{m,op}} e_{s_{m,qr}}} - \overline{n_{c_{m,ij}} e_{s_{m,kl}} e_{s_{m,op}} n_{c_{m,qr}}} -$$
$$\overline{e_{s_{m,ij}} n_{c_{m,kl}} n_{c_{m,op}} e_{s_{m,qr}}} + \overline{e_{s_{m,ij}} n_{c_{m,kl}} e_{s_{m,op}} n_{c_{m,qr}}} -$$
$$\overline{e_{c_{m,ij}} n_{s_{m,kl}} n_{s_{m,op}} e_{c_{m,qr}}} + \overline{e_{c_{m,ij}} n_{s_{m,kl}} e_{c_{m,op}} n_{s_{m,qr}}} +$$
$$\overline{n_{s_{m,ij}} n_{c_{m,kl}} n_{s_{m,op}} n_{c_{m,qr}}} + \overline{n_{c_{m,ij}} n_{s_{m,kl}} n_{c_{m,op}} n_{s_{m,qr}}} . \quad (2.42)$$

Notice that we also assumed that (1) signal and noise are independent, (2) noise samples are independent from element to element and from look to another, and (3) the two orthogonal noise components n_c and n_s are uncorrelated [9].

Now, depending on the relationship between the four elements involved in the two correlation measurements at hand, we recognize five distinct cases that cover all possibilities:

Case 1: Same Element Pair

In this case, we have

$$(i,j) = (o,p) .$$
$$(k,l) = (q,r) . \quad (2.43)$$

Therefore, (2.42) reduces to

$$\overline{\tilde{b}^2_{ij,kl}} = \frac{1}{M}\left[\overline{e^2_{s_{ij}} e^2_{c_{kl}}} - 2\,\overline{e_{s_{ij}} e_{c_{ij}} e_{c_{kl}} e_{s_{kl}}} + \right.$$
$$\overline{e^2_{c_{ij}} e^2_{s_{kl}}} + \overline{n^2_{s_{ij}} e^2_{c_{kl}}} + \overline{n^2_{c_{ij}} e^2_{s_{kl}}} + \overline{e^2_{s_{ij}} n^2_{c_{kl}}} +$$
$$\left.\overline{e^2_{c_{ij}} n^2_{s_{kl}}} + \overline{n^2_{s_{ij}} n^2_{c_{kl}}} + \overline{n^2_{c_{ij}} n^2_{s_{kl}}}\right] . \quad (2.44)$$

We can use the identity

$$\overline{x_1 x_2 x_3 x_4} = \overline{x_1 x_2}\;\overline{x_3 x_4} + \overline{x_1 x_3}\;\overline{x_2 x_4} + \overline{x_1 x_4}\;\overline{x_2 x_3} \quad (2.45)$$

for zero mean Gaussian random variables, [9], to reduce (2.44) to

$$\overline{\tilde{b}^2_{ij,kl}} = \frac{1}{2M}\left[\left[R(0,0) + \sigma_n^2\right]^2 - R^2_{ij,kl}\right] . \quad (2.46)$$

where we used

$$\overline{n_c^2} = \overline{n_s^2} = \frac{1}{2}\sigma_n^2 ,$$
$$\overline{e_c^2} = \overline{e_s^2} = \frac{1}{2}R(0,0) .$$
$$\overline{e^2_{c_{ij}} e^2_{c_{kl}}} = \overline{e^2_{s_{ij}} e^2_{s_{kl}}} = \frac{1}{2}R_{ij,kl} .$$
$$\overline{e_c e_s} = 0 . \quad (2.47)$$

The assumption that e_c and e_s are zero mean Gaussian random variables is well justified according to the central limit theorem [9]. The complex signal received at each array element is the result of a summation of contributions from a large number of scatterers each of which produces a random component with zero mean.

Now, we are in a position to write the diagonal entries of $\mathcal{R}_{\mathcal{I}}$ as

$$\overline{\delta\psi^2_{ij,kl}} = \frac{\overline{\tilde{b}^2_{ij,kl}}}{|R_{ij,kl}|^2} = \frac{1}{2M}\left[\left(\frac{R(0,0)+\sigma_n^2}{R_{ij,kl}}\right)^2 - 1\right], \tag{2.48}$$

which is identical to (2.29).

Case 2: Shared Front Elements

In this case, we have

$$\begin{aligned}(i,j) &= (o,p)\,,\\ (k,l) &\neq (q,r)\,.\end{aligned} \tag{2.49}$$

Therefore, (2.42) reduces to

$$\overline{\tilde{b}_{ij,kl}\,\tilde{b}_{ij,qr}} = \frac{1}{2M}\left[\left[R(0,0)+\sigma_n^2\right]R_{kl,qr} - R_{ij,kl}\,R_{ij,qr}\right], \tag{2.50}$$

and hence

$$\overline{\delta\psi_{ij,kl}\,\psi_{ij,qr}} = \frac{1}{2M}\left[\frac{\left[R(0,0)+\sigma_n^2\right]R_{kl,qr} - R_{ij,kl}R_{ij,qr}}{R_{ij,kl}\,R_{ij,qr}}\right]. \tag{2.51}$$

Case 3: Shared Back Elements

In this case, we have

$$\begin{aligned}(i,j) &\neq (o,p)\,.\\ (k,l) &= (q,r)\,.\end{aligned} \tag{2.52}$$

Therefore, (2.42) reduces to

$$\overline{\tilde{b}_{ij,kl}\,\tilde{b}_{op,kl}} = \frac{1}{2M}\left[\left[R(0,0)+\sigma_n^2\right]R_{ij,op} - R_{ij,kl}\,R_{op,kl}\right], \tag{2.53}$$

and hence

$$\overline{\delta\psi_{ij,kl}\,\psi_{op,kl}} = \frac{1}{2M}\left[\frac{\left[R(0,0)+\sigma_n^2\right]R_{ij,op} - R_{ij,kl}R_{op,kl}}{R_{ij,kl}\,R_{op,kl}}\right]. \tag{2.54}$$

Case 4: Back Element of One Measurement is the Front Element of the Other

In this case, we have

$$\begin{aligned}(k,l) &= (o,p)\,.\\ (i,j) &\neq (q,r)\,.\end{aligned} \tag{2.55}$$

Therefore, (2.42) reduces to

$$\overline{\tilde{b}_{ij,kl}\,\tilde{b}_{kl,qr}} = \frac{-1}{2M}\left[\left[R(0,0)+\sigma_n^2\right]R_{ij,qr} - R_{ij,kl}\,R_{kl,qr}\right]\,, \tag{2.56}$$

and hence

$$\overline{\delta\psi_{ij,kl}\,\psi_{kl,qr}} = \frac{-1}{2M}\left[\frac{\left[R(0,0)+\sigma_n^2\right]R_{ij,qr} - R_{ij,kl}R_{kl,qr}}{R_{ij,kl}\,R_{kl,qr}}\right]\,. \tag{2.57}$$

Case 5: No Shared Elements

In this case, (2.42) reduces to

$$\overline{\tilde{b}_{ij,kl}\,\tilde{b}_{op,qr}} = \frac{1}{2M}\left[R_{ij,op}\,R_{kl,qr} - R_{ij,qr}\,R_{kl,op}\right]\,, \tag{2.58}$$

and hence

$$\overline{\delta\psi_{ij,kl}\,\psi_{op,qr}} = \frac{1}{2M}\left[\frac{R_{ij,op}\,R_{kl,qr} - R_{ij,qr}R_{kl,op}}{R_{ij,kl}\,R_{op,qr}}\right]\,. \tag{2.59}$$

2.3.4 Phase Unwrapping of Correlation Measurements

The least squares solutions represented by equations (2.17) and (2.31) can be rewritten as

$$\underline{\delta}_{\rm ls} = W_{\rm ls}\underline{\Psi}\,. \tag{2.60}$$

$$\underline{\delta}_{\rm mv} = W_{\rm mv}\underline{\Psi}\,. \tag{2.61}$$

where $W_{\rm ls}$ and $W_{\rm mv}$ are the $N_u \times N_e$ matrices given by

$$W_{\rm ls} = (A^T A)^{-1}A^T\,. \tag{2.62}$$

$$W_{\rm mv} = (A^T \mathcal{R}_{\mathcal{I}}{}^{-1} A)^{-1}A^T\mathcal{R}_{\mathcal{I}}{}^{-1}\,. \tag{2.63}$$

and N_u is modified from (2.7) to

$$N_u = NM \tag{2.64}$$

in order to account for distributing the phase reference within the array according to our symmetric phase constraint.

W_{ls} and W_{mv} can be interpreted as weighting matrices applied to the vector of phase measurements, $\underline{\Psi}$, in order to obtain the required phase correction at each array element in the form of a weighted average of all phase measurements. Because of the modulo 2π nature of phase measurements, averaging phase can be quite hazardous [10,11]. In the presence of 2π ambiguities, each phase correction will have an added phase term of the form

$$\gamma_{ij} = \sum_{k=1}^{N_e-1} w_{k,ij} \times 2\pi n_k \,, \tag{2.65}$$

where $w_{k,ij}$ is a fraction, and n_k is an integer ($\{w_{k,ij}\}$ are entries of either W_{ls} or W_{mv}). Therefore, γ_{ij} (modulo 2π) will be a more-or-less random fraction of 2π that varies from one array element to another, and hence will destroy array coherence. Removing 2π ambiguities, or "phase unwrapping" of $\underline{\Psi}$ is essential before applying the weighting matrices as prescribed by (2.60) and (2.61).

We developed a reliable phase unwrapping scheme that allows us to obtain the optimal solution $\underline{\delta}_{\text{mv}}$ (or the suboptimal solution $\underline{\delta}_{\text{ls}}$) with high probability. The main idea is to compare $\underline{\Psi}$ to another vector $\underline{\hat{\Psi}}$ obtained from an available solution $\underline{\hat{\delta}}$, so that 2π ambiguities can be recognized and removed. Entries of $\underline{\hat{\Psi}}$ are computed according to

$$\hat{\psi}_{ij,kl} = \hat{\delta}_{ij} - \hat{\delta}_{kl} \,, \tag{2.66}$$

where $\{\hat{\delta}_{ij}\}$ are entries of $\underline{\hat{\delta}}$ which can be obtained in a number of ways ($\{\hat{\delta}_{ij}\}$ are forced to range between $-\pi, +\pi$ to start with by adding or subtracting the appropriate multiple of 2π to each of them). In the following, we describe a sequential scheme that makes it possible to obtain a near-optimal solution $\underline{\hat{\delta}}$ that allows us to perform the required phase unwrapping and hence obtain the optimal solution $\underline{\delta}_{\text{mv}}$.

To illustrate, let us introduce two quick, suboptimal solutions where one element at the center of a cluster of nearest neighbor elements is considered as a phase reference. The first solution takes the phases of the correlation measurements between this central element and its nearest neighbors as the needed corrections. No phase unwrapping is needed for this cluster. Figure 2.6.a illustrates the situation. The second solution obtains a number of estimates for the same phase correction at each element at the periphery of the cluster. These estimates are obtained by integrating (summing) phase differences over a number of short paths leading to the central element in a way similar to that used in the one-dimensional SCA. Estimates of the same phase correction at each peripheral element are averaged in order to obtain an estimate of improved quality (lower variance).

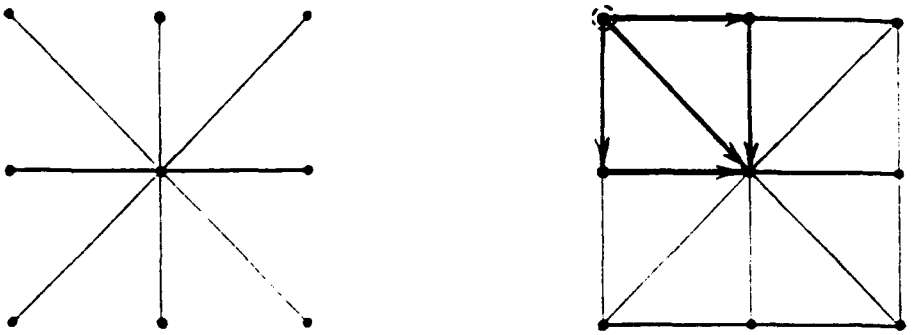

(a) (b)

Figure 2.6. Suboptimal solutions are obtained for a cluster of array elements. Center element is taken as a phase reference. (a) First-neighbor phase differences provide a solution. (b) Another solution is obtained by averaging integrated differences over a number of paths (solid lines).

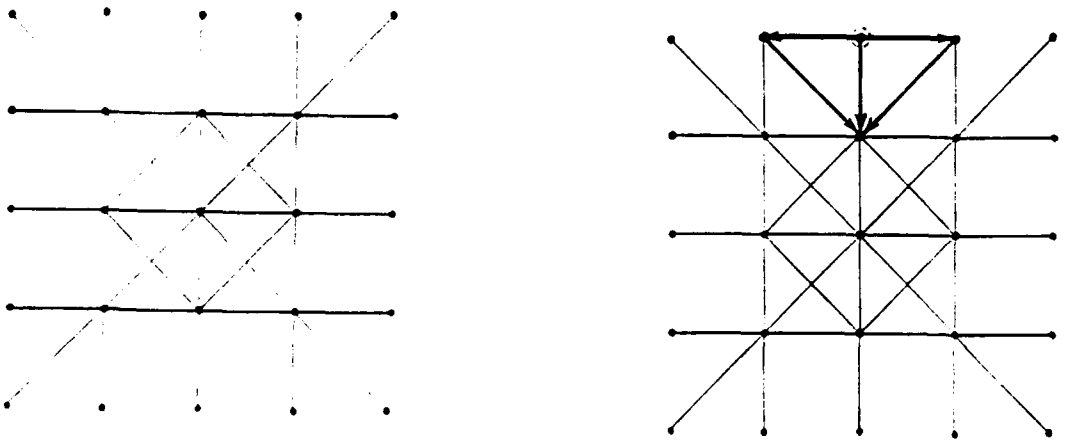

(a) (b)

Figure 2.7. Another layer of elements is included. (a) First-neighbor phase differences provide a solution. (b) Another solution is obtained by averaging integrated differences over a number of paths (solid lines).

To perform the averaging, phase unwrapping is needed. However, unwrapping is trivial since all values being averaged (at each peripheral element) are estimates of the same quantity. 2π ambiguities are easily recognized and corrected. The situation is illustrated in Figure 2.6.b. Notice also that the "phasor method" for phase unwrapping [12,13] could be easily implemented for this purpose. The main idea behind this method is to use the approximation

$$\frac{1}{L}\sum_{l=1}^{L}\phi_l \approx \arg\left\{\sum_{l=1}^{L} e^{j\phi_{a_l}}\right\} = \arg\left\{\sum_{l=1}^{L} e^{j(\phi_l+2\pi n_l)}\right\}, \tag{2.67}$$

where $\{\phi_{a_l}\}$ is a set of ambiguous phase measurements, and $\{n_l\}$ are integers that vary from one term to another. The above approximation holds under the assumption that $\{\phi_l\}$, the unambiguous phase terms, are clustered around some mean value ($\{\phi_l\}$ are allowed to vary around their mean over an interval smaller than π, otherwise the approximation rapidly fails).

Starting from the answers provided by either of our two quick solutions (preferably the second), complete phase unwrapping of all correlation measurements (within the cluster) is performed as mentioned above. Now, the optimal solution for this cluster is obtained according to the weighted least squares method. With the optimal solution for the central cluster in hand, we can progress to the next outward layer of elements. First we obtain a quick answer based on one of our two methods. A generalization of the first method estimates corrections at the new layer by adding the phase differences (from nearest-neighbor correlation measurements) between the new layer and the layer that precedes it to the optimal corrections obtained for that preceding layer (see Figure 2.7.a). A generalization to the second method averages a number of estimates of the differential phase correction needed for each element of the new layer. These estimates are obtained for each peripheral element by integrating phase differences along short paths starting from the same element and ending at that element of the preceding layer nearest to it. As mentioned above, straightforward phase unwrapping is performed before averaging (see Figure 2.7.b). Once more, corrections at the new layer are obtained by adding these smoothed phase differences to the optimal corrections obtained for the preceding layer.

Again, complete phase unwrapping is obtained based on one of our quick solutions. The optimal solution for all elements (up to the new layer) is then obtained. The same procedure is repeated, progressing to outer layers of the array, until the optimal solution for all array elements is reached.

It is worthwhile to notice the following:

(1) The above describes a sequential method for achieving the optimal solution $\underline{\delta}_{\mathrm{mv}}$ where we grow the solution in steps. In each step we increase the size of our

element cluster by including a new layer of elements moving outwards. We try not to deviate much from the optimal solution in each step by using near-optimal solutions only to enable phase unwrapping and then computing the optimal solution for the new cluster. Such a lengthy procedure is only needed when we try to push the system to its limits (considering situations of poor SNR, low spatial correlation, and/or small numbers of looks. For situations where the quality of the phase measurements is moderate to start with, we can obtain a solution, $\underline{\hat{\delta}}$, rather quickly by integrating phase differences staring from a reference element at the middle of the array and moving outwards towards the outer layer of array elements in just one step. $\underline{\hat{\delta}}$ can then be used to phase unwrap $\underline{\Psi}$ in order to obtain $\underline{\delta}_{\mathrm{mv}}$ for the whole array in a second and final step.

(2) We referred to the "phasor method" of phase unwrapping with regard to the possibility of using it to obtain our second "quick" solution (Figures 2.6.b, 2.7.b). The same method can be used in order to obtain a good approximation to $\underline{\delta}_{\mathrm{mv}}$ as well. Caution is due however. Trying to compute entries of $\underline{\delta}_{\mathrm{mv}}$ as

$$\delta_{ij_{\mathrm{mv}}} \approx \arg\left\{ \sum_{k=1}^{N_e-1} |w_{k,ij}| e^{j\,\mathrm{sign}(w_{k,ij})\psi_k} \right\}, \tag{2.68}$$

where ψ_k is the k *th* entry of $\underline{\Psi}$, will fail because $\{\psi_k\}$ are not necessarily clustered within a π interval as required (notice that sign(x) is defined as $\mathrm{sign}(x) = +1, \quad x \geq 0$; $\mathrm{sign}(x) = -1, \quad x < 0$).

A solution on the form of

$$\Delta\delta_{ij_{\mathrm{mv}}} \approx \arg\left\{ \sum_{k=1}^{N_e-1} |w_{k,ij}| e^{j\,\mathrm{sign}(w_{k,ij})[\psi_k - \hat{\psi}_k]} \right\}, \tag{2.69}$$

where $\{\hat{\psi}_k\}$ are entries of $\underline{\hat{\Psi}}$, is possible. In this case, we compute entries of $\underline{\delta}_{\mathrm{mv}}$ as

$$\delta_{ij_{\mathrm{mv}}} \approx \Delta\delta_{ij_{\mathrm{mv}}} + \hat{\delta}_{ij}\,, \tag{2.70}$$

where $\{\hat{\delta}_{ij}\}$ are the suboptimal phase corrections used to compute $\underline{\hat{\Psi}}$ according to (2.66).

Because (2.69) is only an approximate relationship, we found that (2.70) does not converge to the minimum variance solution in just one step. However, we found that updating $\underline{\hat{\Psi}}$ using (2.70) and repeating (2.69) a number of times does converge to the optimal solution after a relatively small number of iterations. This procedure proved to be the most reliable way of reaching the optimal answer under poor operating conditions (low SNR, weak spatial correlation, and/or small number of looks). It should be noted that such an iterative procedure is not computationally intensive because the optimal weights $\{w_{k,ij}\}$, or

simply W_{mv}, need to be computed just once. The same weights are repeatedly applied, according to (2.69), in each iteration.

2.4 Expected Performance

2.4.1 Output Covariance Matrices

The key to predicting the performance of our algorithms is to compute the output covariance matrices $\mathcal{R}_{\mathcal{O}_{\mathrm{ls}}}$ and $\mathcal{R}_{\mathcal{O}_{\mathrm{mv}}}$, defined as

$$\mathcal{R}_{\mathcal{O}_{\mathrm{ls}}} = E\left\{\underline{\delta}_{\mathrm{ls}}\underline{\delta}_{\mathrm{ls}}^T\right\}, \tag{2.71}$$

$$\mathcal{R}_{\mathcal{O}_{\mathrm{mv}}} = E\left\{\underline{\delta}_{\mathrm{mv}}\underline{\delta}_{\mathrm{mv}}^T\right\}. \tag{2.72}$$

Here, $\underline{\delta}_{\mathrm{ls}}$ and $\underline{\delta}_{\mathrm{mv}}$ are the least squares and minimum variance solutions respectively, assuming broadside illumination and the absence of any array distortion. That is, $\underline{\delta}_{\mathrm{ls}}$ and $\underline{\delta}_{\mathrm{mv}}$, in (2.71) and (2.72), reflect only the errors in the estimation process. Therefore, we can write

$$\underline{\delta}_{\mathrm{ls}} = W_{\mathrm{ls}}\delta\underline{\Psi}, \tag{2.73}$$

$$\underline{\delta}_{\mathrm{mv}} = W_{\mathrm{mv}}\delta\underline{\Psi}. \tag{2.74}$$

Substituting (2.73) and (2.74) into (2.71) and (2.72) respectively, expanding W_{ls} and W_{mv} according to (2.62) and (2.63), and using (2.35), we get

$$\mathcal{R}_{\mathcal{O}_{\mathrm{ls}}} = \sigma^2(A^TA)^{-1}, \tag{2.75}$$

$$\mathcal{R}_{\mathcal{O}_{\mathrm{mv}}} = (A^T\mathcal{R}_{\mathcal{I}}{}^{-1}A)^{-1}. \tag{2.76}$$

Notice that we used

$$\mathcal{R}_{\mathcal{I}} = \sigma^2 I \tag{2.77}$$

in deriving (2.75), where σ^2 is the common variance of the presumably uncorrelated phase measurements. As mentioned earlier (with regard to establishing the motivation for deriving the minimum variance solution) equation (2.77) could constitute a gross approximation to the true input covariance matrix, $\mathcal{R}_{\mathcal{I}}$. As we show below, (2.75) results in over-optimistic performance predictions that do not measure up to computer simulation results. Computer simulations have shown the superiority of the minimum variance solution, (2.31), over least squares, (2.17), and verified the accuracy of our performance predictions based on (2.76).

2.4.2 Expected Mainbeam Gain Loss

It is shown in [1,2] that the normalized expected mainbeam gain loss is given by

$$G_o = \frac{1}{N_u} + \frac{2}{N_u^2} \sum_{n>m}^{N_u} \sum_{m=1}^{N_u-1} e^{-\frac{1}{2}[r_{nn}+r_{mm}-2r_{nm}]}. \tag{2.78}$$

where N_u is the total number of array elements given by (2.64), and r_{nm} is given by either

$$r_{nm} = \mathcal{R}_{\mathcal{O}_{\rm ls}}(n,m) \tag{2.79},$$

or

$$r_{nm} = \mathcal{R}_{\mathcal{O}_{\rm mv}}(n,m) \tag{2.80}$$

depending on which solution we are considering.

Concerning ourselves with the minimum variance solution (weighted least squares), we substituted (2.80) into (2.78) in order to produce the set of performance curves shown in Figure 2.8, where we plot G_o versus SNR for different system parameters (SNR refers to the signal to noise ratio per array element). The upper group of curves corresponds to a total of 100 looks. The lower group corresponds to 20 looks. Curves within each group correspond to array sizes 2×2, 3×3, 4×4, and 5×5 (moving from top to bottom).

Performance curves (Figure 2.8) show that a 5×5 array trying to image an extended target (consisting of 3×3 speckles) at a signal to noise ratio of 0 dB per element per look (with a total of 20 available looks) will only suffer a 1 dB loss in the normalized mainlobe gain of its point spread function after applying our optimal solution. Computer simulations verified this result. To the best of our knowledge, such performance is unprecedented (see for example [14]).

Notice that although our computer code is quite general, we can only handle array sizes of up to 5×5 elements because of memory limitations. For an $N \times N$ array, we find that in order to compute $\mathcal{R}_{\mathcal{O}_{\rm mv}}$ (or the optimal weights[†] for that matter), we need to invert $N_e \times N_e$ matrices, where

$$N_e = 4N^2 - 6N + 3.$$

Table 2.1 gives N_e versus N.

[†] Notice that the optimal weights, $W_{\rm mv}$, can be precomputed and stored in a look-up table for a given system. Because the solution is symmetric (due to our symmetric phase constraint) a small fraction of the entries of $W_{\rm mv}$ has to actually be computed and stored.

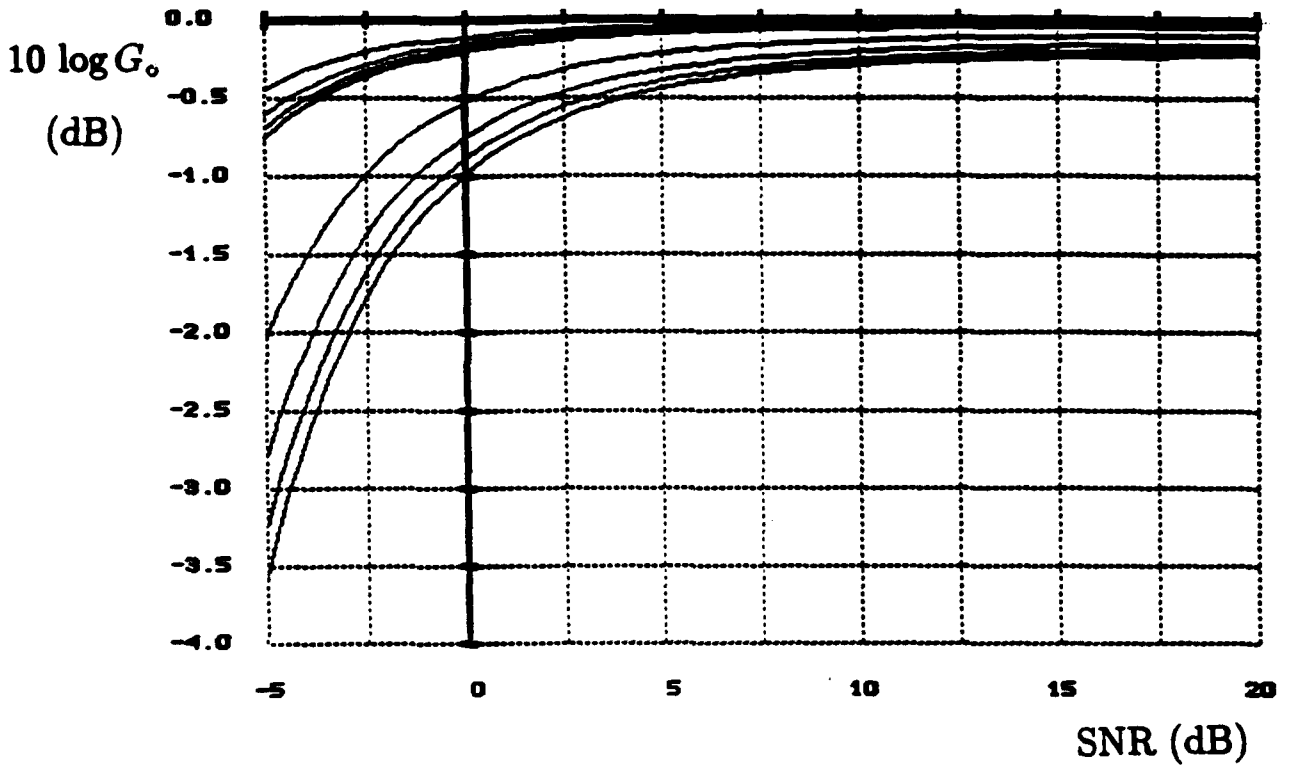

Figure 2.8. Expected normalized mainlobe gain loss (dB) as a function of SNR (dB) for four different array sizes. The upper group of curves corresponds to a total of 100 looks. The lower group corresponds to 20 looks. Curves within each group correspond to array sizes 2×2, 3×3, 4×4, and 5×5 (moving from top to bottom). An extended target is assumed. Target size and interelement spacing are kept constant (in absolute units) for all arrays. For the 5×5 array, target image consists of 3×3 speckles.

Table 2.1. N_e versus N

N	3	5	7	9	11
N_e	21	73	157	273	421

We believe that resorting to more powerful computers (which may be able to barely handle an 11 × 11 array, for example), or complicating the software using our memory-limited machines is beyond the scope of this effort. Our performance curves clearly show the trend for larger array sizes and are, in this sense, quite sufficient.

Finally, we reemphasize the fact that extensive computer simulations have verified all our algorithms and performance predictions.

2.5 References

[1] E.H. Attia, Phase Synchronizing Large Antenna Arrays Using The Spatial Correlation Properties of Radar Clutter, Ph. D. Thesis, The Moore School of Electrical Engineering, University of Pennsylvania, 1984.

[2] E.H. Attia and B.D. Steinberg, "Self-Cohering Large Antenna Arrays Using The Spatial Correlation Properties of Radar Clutter," *IEEE Trans. Antennas and Propagation*, Vol. AP-37, No. 1, pp. 30-38, January 1989.

[3] E.H. Attia, "Phase Synchronizing Large Antenna Arrays Using the Spatial Correlation Properties of Radar Clutter," ***National Radio Science Meeting (URSI)***, Boulder, Colorado, January 1984, Meeting Digest p. 105.

[4] K. Abend, E.H. Attia, B. Fell, E. Stockburger, and H. Subbaram, *Synchronizing and Cohering a Distributed Sparse Array Radar*, Phase II Final Report, SBIR No. AF87-173, Contract No. F04701-88-C-0117, prepared by **Interspec**, Inc. for USAF/SD, January, 1991.

[5] H. Subbaram and B.D. Steinberg, "A Scene-Independent Technique for Self-Calibrating Phased Arrays in a Coherent Target Environment," *Proc. 1987 URSI Radio Science Meeting*, Virginia Polytech. Inst., Blacksburg, VA, June 1987.

[6] B.D. Steinberg and H. Subbaram, *Microwave Imaging Techniques*, John Wiley & Son, New York, 1991.

[7] N. Morrison, *Introduction to Sequential Smoothing and Prediction*, McGraw-Hill, New York, 1969.

[8] G. Golub and C. Van Loan, *Matrix Computations*, Johns Hopkins University Press, Baltimore, Maryland, 1983.

[9] J.B. Thomas, *An Introduction to Statistical Communication Theory*, John Wiley & Son, New York, 1969.

[10] E.H. Attia, "Self-Cohering Airborne Distributed Arrays Using the Robust Minimum Variance Algorithm," *IEEE AP-S and URSI International Symposium*, Philadelphia, Symposium Digest, Vol. 2, pp. 603-606, June 1986.

[11] E.H. Attia, *Self Cohering Airborne Distributed Arrays*, **Interspec** final report on contract No. F10628-C-0080 for Rome Air Development Center, Hanscom, MA, December 1985.

[12] H. Takajo and T. Takahashi, "Least Squares Phase Estimation from the Phase Difference," *J. Opt. Soc. Am. A*, Vol. 5, pp. 416-425, March 1988.

[13] P. Nisenson, "Speckle Imaging with the PAPA Detector and the Knox-Thompson Algorithm," in *Diffraction-Limited Imaging with Very Large Telescopes*, D.M. Alloin and J.M. Mariotti, eds., Kluwer, Boston, 1989, pp. 157-169.

[14] J. Cederquist, J. Fienup, J. Marron, T. Schultz, and J. Seldin "Digital Shearing Laser Interferometry for Heterodyne Array Phasing," *Proc. SPIE*, Vol. 1416, pp. 266-277, 1991.

[15] S. Clark, L. Jones, and L. DeSandre, "Coherent Array Optical Imaging," *Appl. Opt.*, Vol. 30, pp. 1804-1810, 1991.

3.0 PHASE II EXPERIMENTS

3.1 Equipment Definition

We identified two practical possibilities for the experimental validation of our self-cohering techniques. Each possibility has its attractive features. In the following we discuss both.

3.1.1 Using NWC Experimental System

Figure 3.1 shows the basic experimental system at the Naval Weapons Center (NWC), China Lake, California [1,2]. The following is a brief description of the system based on [2]. The experimental set-up consists of a Mach-Zender interferometer as shown in Figures 3.1.a and 3.1.b. Initially, homodyne detection was implemented at NWC: i.e., both the laser and local oscillator (LO) were of the same frequency. To obtain accurate measurements of the complex amplitude of the signal in the homodyne mode, quadrature detection was used by recording two interference patterns where the second one was 90° out of phase with the first. This phase change was performed by mounting mirror M (Figure 3.1.a) on a PZT and changing the PZT voltage so as to translate the mirror $\lambda/8$.

To enable the effects of Doppler shifts to be studied and thereby demonstrate improved resolution, the set-up was modified to that shown in Figure 3.1.b. The two signal beams are, respectively, reflected off of PZT-mounted mirrors once or twice. The Doppler shifts are introduced by ramping the PZT mounted mirrors in unison with the result that if the beam reflecting off only one PZT-mounted mirror has a shift f, the beam reflecting off both PZT-mounted mirrors has a shift of $2f$. Since in this mode of operation the interference pattern can now be monitored as a function of time, quadrature detection is not required. Instead, one interference pattern coupled with the temporal information is enough to extract the complex amplitude of the signal.

Due to electronic simplicity and the size and number of its detectors, a CCD video camera is used. The size of each detector aperture ($\approx 20 \times 20$ μm) results in high mixing efficiency between the signal and LO beams over laboratory distances, while the large number of detectors allows arrays as large as 127 x 127 elements. A major disadvantage of the CCD is its low frequency response (< 15 Hz). Although low, this bandwidth is enough to use with very low frequency Doppler shifts and thereby emulate a real (high speed) system. For example, a slowly rotating turntable is often used in order to either resolve an extended target (mounted on top of the turntable) in Doppler, or provide a number of independent looks of such a target provided that the target has an optically-rough (diffuse) surface. The video camera is linked to a computer-controlled video frame grabber that enables

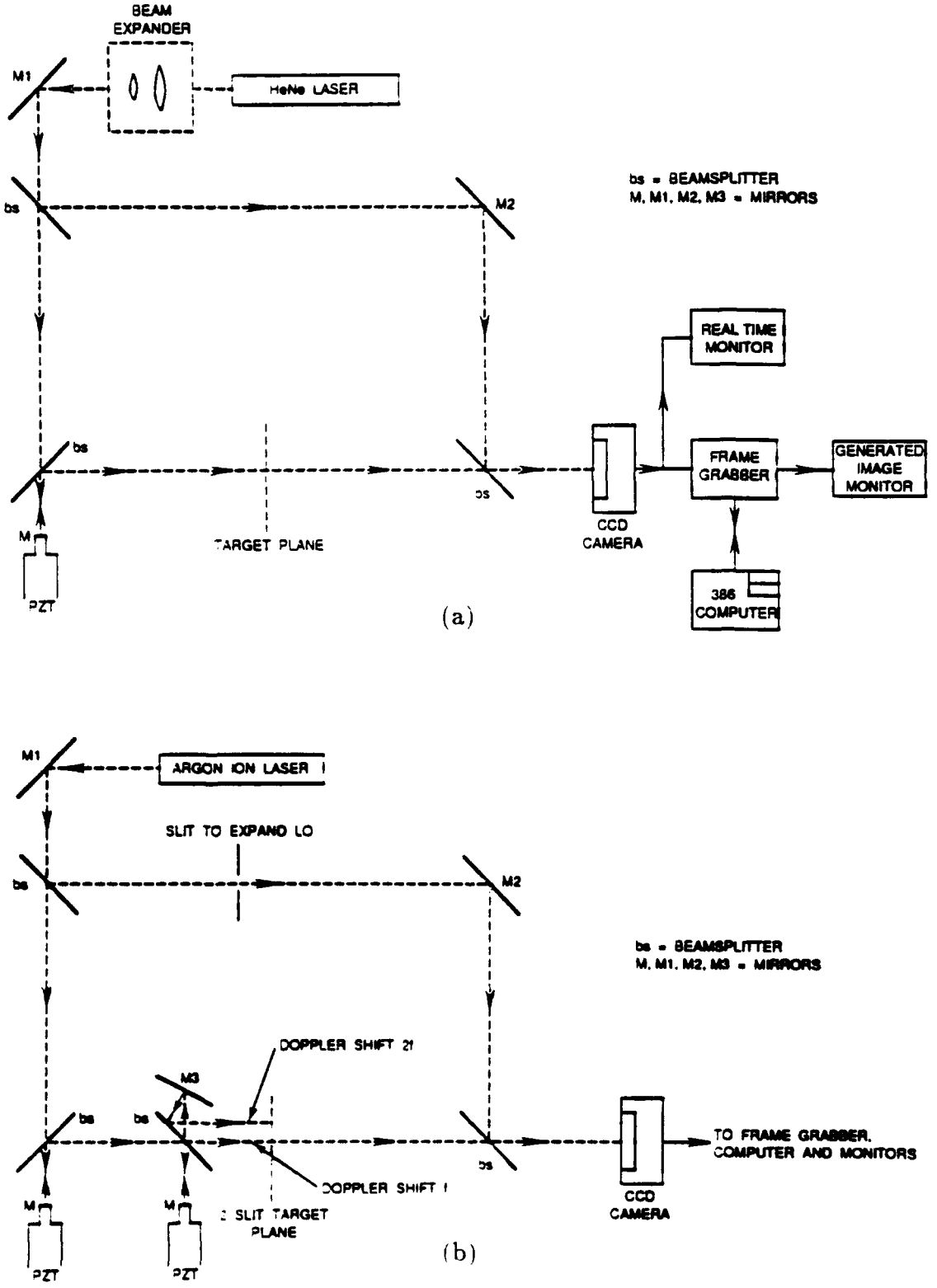

Figure 3.1. Experimental configuration at NWC. (a) angle-angle imaging. (b) angle-angle-Doppler imaging (From [2]).

acquisition and subsequent processing of the data. No lenses are attached to the camera. Instead, light is allowed to fall directly onto the photosensitive surface.

Since the positions of the photodetectors fall on an optically-precise rectangular grid fixed on the CCD chip, aberrations are primarily introduced by ensuring that the mirror $M2$ in Figures 3.1.a and 3.1.b is of very low quality, introducing about three waves of errors by the LO. Further aberrations are introduced by inserting a piece of frosted bathroom glass in the LO beam.

Notice that the most attractive feature of the experimental system at NWC is that it already exists. A number of useful experiments can be performed using this existing set-up with virtually no added cost in terms of investments in new hardware. On the other hand, the existing system is restrictive in many important respects. Most restrictions stem from the fact that the receive array is made of a CCD chip. As mentioned above, such a CCD array has a very low bandwidth and offers no significant geometrical flexibility. In order to overcome these shortcomings, we introduce the following alternative experimental system.

3.1.2 A 10×10 Experimental Array

The second practical possibility is to build a flexible experimental array system consisting of individual detectors (photo-diodes) of a useful, but yet economical, size. We propose to build a 10×10 heterodyne array of individual detectors in the visible region. Such an array can produce useful angle-angle images of extended targets (resolving them into 5×5 pixels for example). Moreover, working in the visible region obviates the need for expensive liquid nitrogen cooling, which would be required for an infra-red (CO_2 laser) system. Data collection will be PC-based using off-the-shelf multi-channel A/D conversion cards (with bus extension units). This strategy will minimize development cost. Figure 3.2 illustrates the proposed system. A cw Argon Ion laser will be used to illuminate a very slowly rotating target. The PZT-mounted mirror, M, is used to introduce a constant doppler shift in the LO signal (reflected off its surface) by ramping the voltage across the PZT during data collection. This frequency shift is needed in order to separate the complex amplitude of the received signals by digital filtering without the need for quadrature detection. The introduced shift in LO frequency should be greater than (or equal to) the maximum doppler shift due target rotation. Therefore, the minimum needed sampling rate should be equal to twice the target doppler bandwidth (for a symmetric target, doppler bandwidth will be equal to twice the maximum doppler shift in target returns). Our proposed data acquisition system will enable us to sample the receive aperture at a 250 k sample/sec rate. Such a sampling rate (which is much higher than that of any experimental set-up in existence) will allow us to study self-phasing in the presence of atmospheric turbulence and array vibrations.

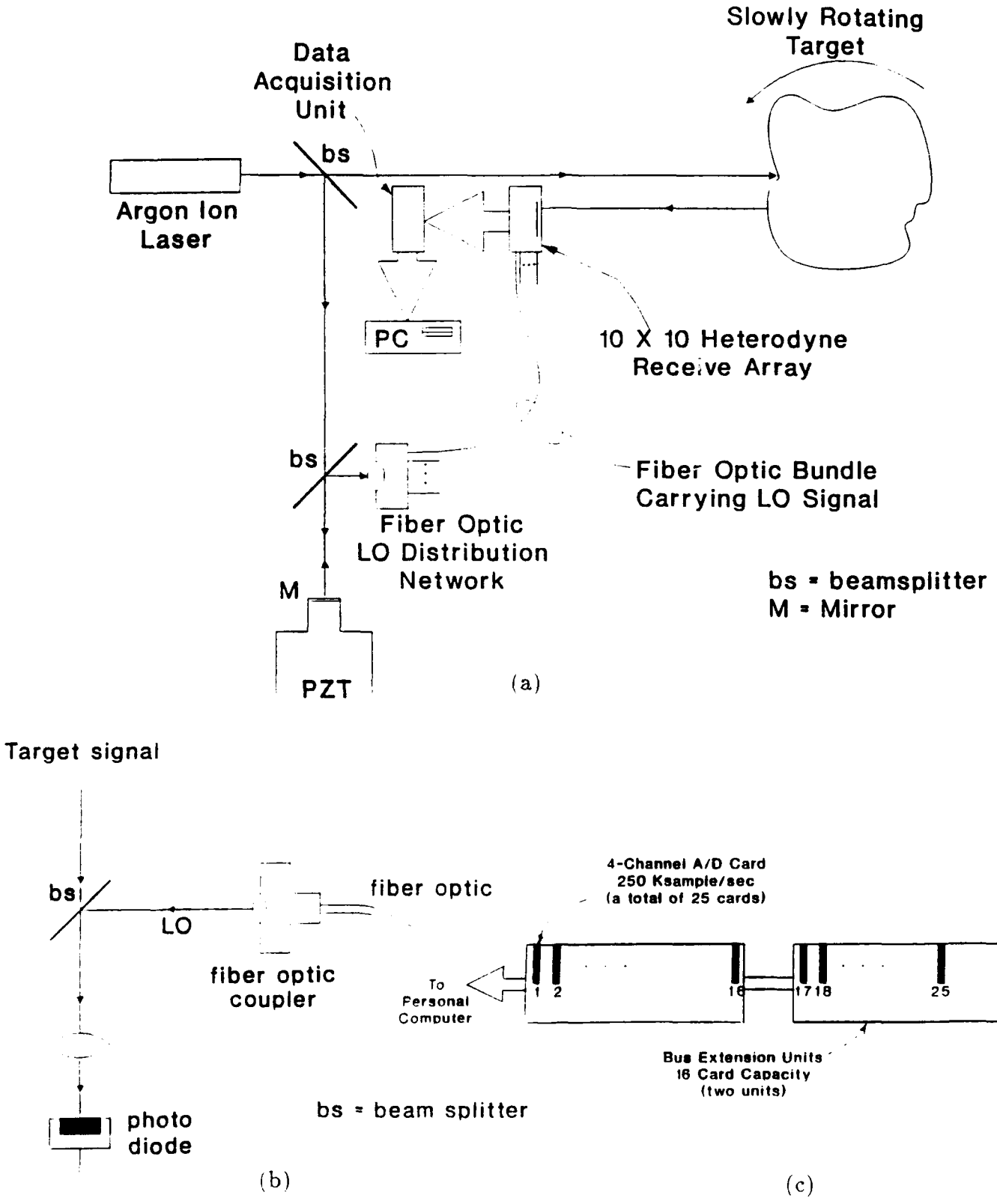

Figure 3.2. A proposed 10 x 10 array of individual detectors. (a) experimental configuration. (b) array element. (c) data acquisition.

Compared with existing experimental systems [1-3], which use unaberrated, monolithic CCD detector arrays (obtained from commercially available video cameras), our proposed set-up will offer the following:

(1) The ability to introduce true mechanical errors (axial errors, etc.).

(2) The ability to experiment with different array geometries (highly thinned, random, rectangular, square, linear, etc.).

(3) The ability to introduce vibrations within the array. This can simulate an airborne system (above the clouds) for a Theater Missile Defense (TMD) scenario.

(4) The ability to image a small target at a longer range through significant atmospheric turbulence using a large, thinned array configuration (simulating a practical TMD scenario). Such an experiment is possible because photo-diodes offer significantly higher bandwidths (compared to CCD arrays). Notice that time-varying atmospheric turbulence can be emulated using a fan or a blow-torch.

(5) The ability to upgrade the working bandwidth of the system by upgrading the data acquisition and data transfer systems.

An initial estimate of the cost of building our proposed experimental system (labor and materials) comes roughly to \$120 K which is well within the Phase II SBIR budget. Table 3.1 provides details of our rough cost estimate.

3.2 Experiments Definition

As discussed above, we are considering two possibilities for the experimental validation of our self-cohering techniques. Definition of the Phase II experiments depends on which of the two systems is going to be used. In the following, we consider both possibilities.

3.2.1 Experiments Performed Using the NWC Set-Up

Using the experimental set-up at NWC (described in Section 3.1.1), we can demonstrate the following self-cohering algorithms and compare their performance as a function of SNR:

(1) Least squares two-dimensional (2-D) SCA.

(2) Weighted least squares (minimum variance) 2-D SCA.

(3) The SCA as a "multiple scatterer algorithm".

Table 3.1. Cost Estimate of the 10 × 10 Experimental Array

Item	Quantity	Unit Price	Price
Ion Argon Laser	1	$10,000	$10,000
Beam Splitters	2	$100	$200
PZT-Mounted Mirror	1	$200	$200
Precision Turntable	1	$2,000	$2,000
Fiber Optic LO Distribution Network	1	$1,000	$1,000
Fiber Optic Bundle	1	$600	$600
Array Elements	100	$400	$40,000
4-Channel A/D Cards	25	$1,000	$25,000
Bus Extension Units	2	$500	$1,000
		Total Material Cost	$80,000
		Labor	$40,000
		Total Cost	$120,000

In (1) and (2), a number of independent looks will be obtained from a slowly rotating, extended, diffuse test target. Correlation measurements will be made based on these independent looks and used to compute either solution. Also, our symmetric phase constraint will be implemented. The following methods of phase-unwrapping (which we developed during the course of this Phase I study) will be tried and compared in terms of reliability (success rate):

(a) Direct phase-unwrapping.

(b) Generalized, iterative phasor method.

The initial solution for array phase corrections needed for (a) and (b) will be obtained according to the following two methods (discussed in Section 2.3.4):

(i) Direct integration of phase differences starting from an element near array center and moving outwards (radially) in all directions (quickest method).

(ii) Sequential near-optimal/optimal solutions for subarrays of growing size (most reliable method).

In (3), returns from a number of scatterers on the surface of a slowly rotating extended test target will be separated according to Doppler and then used to provide the correlation measurements needed by different versions of the two-dimensional SCA.

In all cases, array aberration will be emulated as described in Section 3.1.1. Also, *before* and *after* (self-cohering) images will be produced. Quantitative evaluation of performance will be based on the normalized gain loss of the mainlobe of the point spread function which can be obtained from residual phase errors in the absence of array distortion (see Section 2.4).

3.2.2 Experiments Performed Using the 10×10 Array

In addition to all experiments defined in Section 3.2.1, the 10×10 array will be used to demonstrate the following:

(1) Self-cohering in the presence of true position errors in the array. Axial as well as transversal position errors will be introduced by perturbing the positions of individual detectors from one experiment to another.

(2) Self-cohering in the presence of mechanical vibrations. Such vibrations will be introduced into the simple structure supporting the array using a small dc motor driving an eccentric wheel. Notice that in order to ensure successful dynamic self-cohering, array structure should look "frozen" (on a wavelength scale) during the time it takes to collect the necessary "looks".

(3) Self-cohering in the presence of atmospheric turbulence. A heat source (e.g., a blow-torch) or a fan will be used to introduce significant turbulence in the received signal path. The amount of turbulence will be measured in terms of the ratio D/d_o, where D is the diameter of the true aperture, and d_o is that of the reduced effective aperture (due to turbulence). Similar to self-cohering in the presence of vibrations, data collection must be much faster than turbulence decorrelation time.

(4) Various array geometries such as highly thinned, random, rectangular, square, circular, linear, etc.

3.3 References

[1] S.E. Clark and L.R. Jones (Naval Weapons Center, China Lake, Cal.), "Electronically Combined Coherent Arrays (ECCA) for Laser Radars," a viewgraph presentation given to **Interspec** technical staff, Ambler, PA, May, 1990.

[2] S. Clark, L. Jones, and L. DeSandre, "Coherent Array Optical Imaging," *Appl. Opt.*, Vol. 30, pp. 1804-1810, 1991.

[3] J. Cederquist, J. Fienup, J. Marron, T. Schultz, and J. Seldin "Digital Shearing Laser Interferometry for Heterodyne Array Phasing," *Proc. SPIE*, Vol. 1416, pp. 266-277, 1991.

4.0 CONCLUSIONS AND RECOMMENDATIONS

The main conclusion of this Phase I SBIR study is that "self-phasing" of a large receive array of optical subaprtures is quite feasible using our advanced "self-cohering" techniques. That is, it is possible, for a bistatic laser radar system, to obtain diffraction-limited performance from a badly distorted, large, optical receive aperture adaptively (using returns from the target area). No strong point source is required. Instead, a number of independent "looks" from the target are needed. These looks can be obtained via either of the following two methods (or by a combination of both):

(1) By range diversity. That is, if the laser radar can resolve the target into a number of range cells, then each target range cell will provide us with an independent look.

(2) By rotation diversity. A rotating target with a diffuse surface will provide us with a number of independent looks as we observe it over time. Because of the short optical wavelengths involved, a small rotation from pulse to pulse is sufficient to decorrelate the looks.

During the course of this study, we developed a number of advanced self-cohering techniques suited to the problem. In particular, we developed:

(1) Least squares two-dimensional (2-D) SCA.

(2) Weighted least squares (minimum variance) 2-D SCA.

(3) The SCA as a "multiple scatterer algorithm".

The first two techniques can be considered as extensions of the Spatial Correlation Algorithm (SCA) to two-dimensional array geometries. The second algorithm provides the optimal solution to the problem given a reasonable number of looks. For the case where we have a limited number of looks and some of which contain dominant scatterers, the third technique exploits these special looks in order to achieve effective self-cohering.

All three techniques solve a set of overdetermined equations relating array distortion to phase measurements. The solutions take on the general form

$$\underline{\delta} = W\underline{\Psi}, \tag{4.1}$$

where $\underline{\delta}$ is the vector of phase corrections, W is a weighting matrix, and $\underline{\Psi}$ is the vector of differential phase measurements.

We developed a symmetric phase constraint that resulted in a symmetric solution amenable to fast matrix inversion algorithms (needed for computing W). Notice that the optimal weights, W, can be precomputed and stored in a look-up table for a given system. Because

the solution is symmetric, a small fraction of the entries of W has to actually be computed and stored.

Phase-unwrapping of $\underline{\Psi}$ is essential before applying (4.1). We developed the following methods of phase-unwrapping:

(a) Direct phase-unwrapping.

(b) Generalized, iterative phasor method.

Both methods, (a) and (b), require an initial solution for array phase corrections. We developed two techniques for obtaining such an initial solution (see Section 2.3.4):

(i) Direct integration of phase differences starting from an element near array center and moving outwards (radially) in all directions (quickest method).

(ii) Sequential near-optimal/optimal solutions for subarrays of growing size (most reliable method).

We analyzed and predicted the performance of our newly developed algorithms. Performance predictions are very promising (predicted performance meets and exceeds the goals set by the staff of the Naval Weapons Center (NWC), China Lake, California). Performance curves show that a 5×5 array trying to image an extended target (consisting of 3×3 speckles) at a signal to noise ratio of 0 dB per element per look (with a total of 20 available looks) will only suffer a 1 dB loss in the normalized mainlobe gain of its point spread function after applying our optimal solution. Computer simulations verified this result. To the best of our knowledge, such performance is unprecedented.

In general, extensive computer simulations have verified all our algorithms and performance predictions.

We have also designed two sets of Phase II experiments for the purpose of demonstrating our advanced self-cohering techniques:

(1) Using the NWC experimental system:

(1.1) A number of useful experiments can be performed with existing hardware.

(1.2) On the other hand, the existing CCD array has a very low bandwidth and offers no significant geometrical flexibility.

(2) Building a 10×10 array of individual detectors. This approach makes it possible to test our techniques under realistic conditions. Such an experimental set-up will enable us to:

(1) Introduce true mechanical errors.

(2) Experiment with different array geometries.

(3) Introduce vibrations within the array. This can simulate an airborne system (above the clouds) for a Theater Missile Defense (TMD) scenario.

(4) Image a target through significant atmospheric turbulence (for possible TMD applications).

(5) Upgrade the working bandwidth of the system by upgrading the data acquisition and data transfer systems.

For future work, we recommend the following:

(1) Build the 10×10 array experimental system described in Section 3.1.2, and use it in order to demonstrate the validity and performance of our advanced self-cohering techniques under realistic conditions. In particular, we recommend to perform all experiments defined in Section 3.2 for our proposed flexible experimental set-up.

(2) Develop fast algorithms to compute the optimal weights. A number of subarray processing ideas should also be pursued. For example, the optimal weighting matrix for a smaller subarray could be used throughout the larger array provided some overlap between subarrays is allowed [1].

(3) Perform some theoretical work aimed at comparing the performance with and without the symmetric phase constraint. Our observations indicate that our symmetric phase constraint results in superior performance as well. A theoretical proof is needed however.

4.1 References

[1] E.H. Attia, *Self Cohering Airborne Distributed Arrays*, **Interspec** final report on contract No. F10628-C-0080 for Rome Air Development Center, Hanscom, MA, December 1985.